# Adult Neurogenesis Reconciles Flexibility and Stability of Olfactory Perceptual Memory

Bennet Sakelaris and Hermann Riecke

Engineering Sciences and Applied Mathematics, Northwestern University, Evanston, Illinois, United States of America

March 3, 2024

## Abstract

The abilities to learn and store memories are inherently at odds with each other: the brain must be flexible enough to quickly store new information, but stable enough to avoid overwriting old memories. We show that adult neurogenesis can overcome this flexibility-stability dilemma. We develop a computational model for adult neurogenesis and structural spine dynamics in the olfactory bulb that captures many experimental observations and show that the transient properties of adult-born neurons confer multiple contributions to addressing this problem. First, the enhanced plasticity of young neurons allows them to flexibly encode new memories; as the neurons age, these memories stabilize, while remaining in the same neural ensemble. Second, the young new neurons' enhanced excitability and susceptibility to apoptosis maintain the flexibility of the memory. Finally, the period of sensory-dependent dendritic elaboration establishes an additional substrate of memory that facilitates rapid relearning. The model makes experimentally testable predictions and identifies a new functional role of adult neurogenesis in olfaction: memory consolidation.

## 1 Introduction

Learning and the subsequent retention of the learned information are fundamental tasks of the brain. Here, we focus on perceptual learning where an animal learns to discriminate between similar stimuli through repeated experience. Importantly, this type of learning occurs even in the absence of explicit rewards or aversions that may modulate plasticity. Thus, in this situation the animal faces the flexibility-stability dilemma [Grossberg, 1982], wherein the acquisition of memories should be flexible enough to continually encode new memories while being stable enough that new stimuli do not overwrite old memories.

In the olfactory system perceptual learning has been shown to occur in the olfactory bulb (OB) [Gschwend et al., 2015, McNamara et al., 2008], which is renowned for its high degree of structural plasticity, most notably through adult neurogenesis. The precise purpose of adult neurogenesis is still a matter of debate. Experiments have shown that it is necessary for certain forms of perceptual learning [Moreno et al., 2009, Li et al., 2018], and computational modeling provides some understanding of the underlying mechanisms [Chow et al., 2012, Adams et al., 2019, Shani-Narkiss et al., 2020, Kersen et al., 2022]. However, in principle, these behavioral observations could also be explained by synaptic plasticity alone [Sailor et al., 2016, Meng and Riecke, 2022, Wiechert et al., 2010], leaving the reason for neurogenesis an open question.

Here, using a computational model of the OB, we demonstrate that the flexibility-stability dilemma can be ameliorated through the maturation of adult-born neurons. The heightened excitability and plasticity of newly arrived young cells [Kelsch et al., 2009, Nissant et al., 2009, Wallace et al., 2017] allow them to rapidly store new memories when they are young, and stabilize the memories as the neurons age and become less plastic. We further show that the

transiently increased excitability of new neurons is important for helping them integrate into the network, while on longer time scales, their higher rate of apoptosis is needed to remove unnecessary neurons that would interfere with the ability of newer neurons to integrate when learning new odors.

Our biophysically motivated model captures a host of recent experimental observations, including how adult-born granule cells (abGCs), the primary neurogenic population in the OB, are preferentially recruited to process new odors [Moreno et al., 2009, Forest et al., 2019, Forest et al., 2020], and how the silencing of these abGCs extinguishes memory [Forest et al., 2020]. Additionally, young abGCs are highly sensitive to retrograde interference and die if a new odor pair is presented without the previously presented odor pair still present in the environment [Forest et al., 2019]. Moreover, our model makes multiple experimentally-testable predictions including that the rapid re-learning of a forgotten odor pair [Sultan et al., 2010] is enabled by the sensory input-dependent dendritic elaboration of neurons that initially encoded the odors, and that it would occur even if neurogenesis was blocked following the first enrichment. A further prediction by the model is that long time periods without odor enrichment should negatively impact the subsequent ability to learn new odors.

Furthermore, in systems where both learning and forgetting occur on the same fast time scale the overall memory capacity grows only logarithmically with the number $N$ of synapses [Amit and Fusi, 1994, Fusi and Abbott, 2007]. Our computational model predicts that a network with age-dependent plasticity rates can have a vastly larger memory capacity on the order of $\sqrt{N}$. This emphasizes not only that the augmented capacity of the model predominantly arises from the age-dependent plasticity rates rather than the mere addition of synapses, but also that this framework uses the new synapses provided by adult neurogenesis more efficiently. Moreover, this scaling is equivalent to that of other theoretical models designed to resolve the flexibility-stability dilemma including the cascade model [Fusi et al., 2005] and the partitioned memory system model [Roxin and Fusi, 2013].

# 2 Results

We studied the effects of adult neurogenesis on a structurally constrained neural network that was designed to include many important, specific aspects of the olfactory bulb. Although simpler models could be used to investigate adult neurogenesis, we chose this “bottom-up” approach in the hope that it may uncover specific roles played by adult-born neurons in the OB. This is a particularly important choice to make in order to understand the role of adult neurogenesis in the brain as adult-born neurons mature differently in the olfactory system than the hippocampus [Lledo et al., 2006] and likely play different roles in the two brain areas [Aimone, 2016].

## 2.1 Formulation of the model

We considered an OB network comprising two distinct populations or layers of neurons: the primary layer consisting of excitatory mitral cells (MCs) and the secondary layer composed of inhibitory granule cells (GCs). The MC layer receives sensory input via glomerular activation patterns, thereby forming representations of stimuli in MC activity. These representations are shaped by the reciprocal connections between the MC and GC layers and project to the olfactory cortex for further processing (Figure 1A).

Rather than assuming an exhaustive "all-to-all" connectivity pattern, we incorporated the sparse structural characteristics of the dendritic networks within both the MC and GC populations by randomly selecting a subset of MCs with which each individual GC forms synaptic connections. The MC-GC synaptic network is persistently modified by activity-dependent structural synaptic plasticity in which synapses located on GC dendrites are formed and eliminated. Because such structural plasticity is known to rely on the local calcium concentration at the spine [Kasai et al., 2021], we adopt a previously published model that approximates the calcium concentration at each synapse as a function of pre- and post-synaptic activity [Graupner and Brunel, 2012] (Figure 1B).

We model the synaptic dynamics with a Markov chain consisting of three states: non-existent, unconsolidated, and consolidated (Figure 1C). Non-existent synapses represent lo-

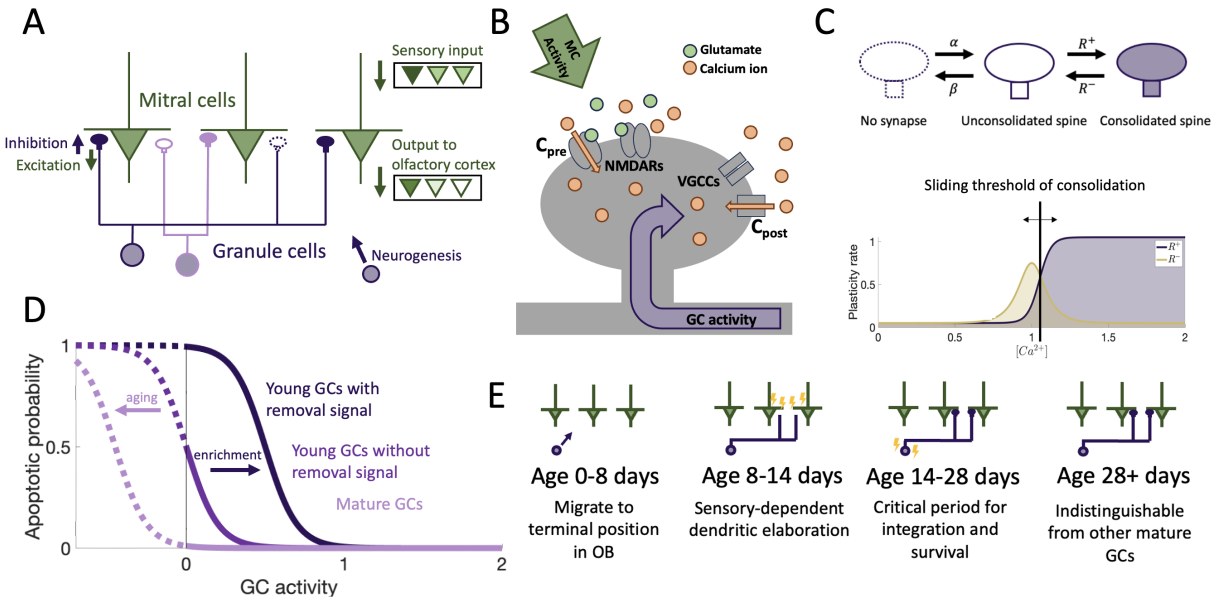


Figure 1: **Computational model.** (A) Network. MCs relay stimuli to cortex. Reciprocal synapses with GCs can be functional or non-functional (cf. C). Adult neurogenesis adds granule cells. (B) Calcium controls synaptic plasticity (cf. [Graupner and Brunel, 2012]). Influx into spine through MC-driven NMDARs and through voltage-gated calcium channels (VGCC) opened by global depolarization of GCs. (C) Spine dynamics. Unconsolidated spines are formed with rate $\alpha$ and removed with rate $\beta$. Spines become consolidated with a rate $R^+$ and deconsolidated with rate $R^-$ (Top). $R^\pm$ depend on the local calcium concentration in the spine (Bottom). (D) Apoptosis. Granule cells are removed with a rate that depends on GC activity, the age of the abGCs, and environmental factors (see Methods). (E) Development of abGCs. At age 8-14 days they integrate silently into the OB. The formation and elaboration of their dendrites depends on sensory input. During their critical period (14-28 days) the abGCs are more excitable and plastic and have a higher rate of apoptosis. Beyond 28 days the abGCs are mature GCs.

cations where a synapse between a MC and GC is geometrically possible but not realized. Unconsolidated synapses represent filopodia, silent synapses, or unconsolidated spines that provide a foundation for a functional synapse but do not yet facilitate a postsynaptic response. Finally, consolidated synapses represent fully functional connections. We assume that synapses transition between the unconsolidated and non-existent states at a constant rate, independently of activity. Conversely, transitions between unconsolidated and consolidated synapses occur with an activity-dependent rate so that sensory experience shapes the connectivity of the network. This assumption arises from experimental findings that GC spine dynamics depend on GC activity [Breton-Provencher et al., 2014, Breton-Provencher et al., 2016, Saha et al., 2021]. In turn, we model these transitions with a rule similar to the Artola-Bröcher-Singer (ABS) rule [Artola et al., 1990, Artola and Singer, 1993] (Figure 1C, see methods) where highly active unconsolidated synapses are more likely to undergo consolidation [Vardalaki et al., 2022] and less active consolidated synapses more likely to undergo deconsolidation [Kasai et al., 2021]. We further assume that each synaptic state is associated with a fixed weight value. Specifically, non-existent and unconsolidated synapses have synaptic weight zero, while consolidated synapses have weight one. We recognize that this approach ignores synaptic weight plasticity, but note that these binary synapses are representative of a class of realistic synaptic models [Fusi, 2021]. Moreover, only limited informatioon is available for the weight plasticity of MC-GC synapses [Gao and Strowbridge, 2009].

Because the OB has been shown to be responsible for perceptual learning [McNamara et al., 2008, Gschwend et al., 2015], we "enrich" the network through repeated alternating presentations of similar artificial stimuli (Figure 2B) and assess its ability to discriminate between these stimuli over the course of training. We confirm that changes in the representations of these similar stimuli in MC activity diverge as a result of training (Figure 2B) and track the memory both as quantified by changes in the MC-GC connectivity as well as the discriminability of the representation of the stimuli in MC activity (see Methods).

## 2.2 Age-dependent plasticity reconciles flexibility and stability

In order to establish what can be gained from the addition of new neurons alone, we initially disregarded apoptosis and the transient properties of abGCs (Figure 1D, E), resulting in a minimal model of adult neurogenesis in the OB where a homogeneous population of GCs grew over time. In Figure 2C we simulated neurogenic (solid lines) and non-neurogenic (dashed lines) networks consisting of uniformly fast (green) and slow (blue) synapses. We observe no difference in the results of the neurogenic and non-neurogenic models in either of the measurements of memory we recorded. Moreover, the highly plastic networks learns and forgets quickly, while the weakly plastic networks learns and forgets slowly, illustrating the flexibility-stability tradeoff.

Due to the pivotal roles of plasticity rates in memory encoding, we first explored the impact of the differing rates of synaptic plasticity in young and old GCs (Figure 2A). We calibrated the rates of spine turnover to align with empirical data [Sailor et al., 2016] (Figure S1). We found this adjustment partially resolved the flexibility-stability dilemma, as the age-dependent network could encode memories more swiftly than the network of weakly plastic synapses while maintaining greater stability than the network with highly plastic synapses (Figure 2C, red curves). Thus the heightened plasticity of young abGCs allows them to rapidly encode new memories and retain them as the neurons matured and their plasticity rate decreased.

To better understand how memories were encoded in the OB, we analyzed the MC-GC connectivity immediately following enrichment. We performed hierarchical clustering on the columns of the connectivity matrix in order to cluster GCs into groups of similar connectivity. We find two distinct clusters: a large portion of GCs maintained their existing, random connectivity (purple in Figure 2D), while others exhibited a preference for forming connections with MCs that responded strongly to the enrichment odors (orange in Figure 2D). Subsequently, we investigated cluster membership based on the birth-date of GCs (Figure 2E). The results clearly show the preferential recruitment of immature abGCs (grey shaded areas) to the learning cluster, while only a small

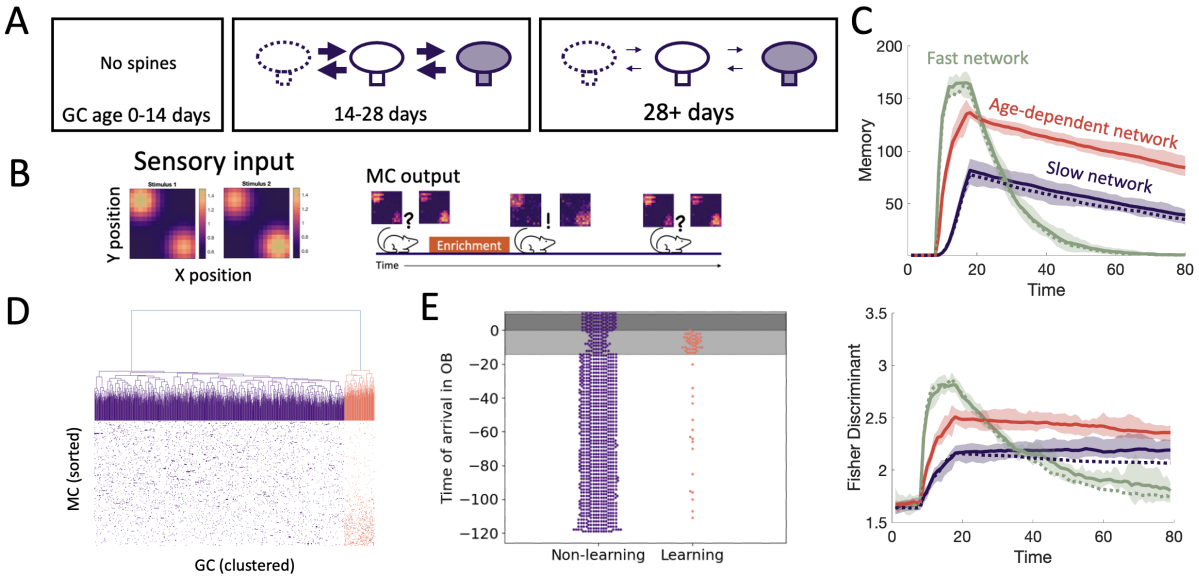


Figure 2: **Age-dependent plasticity.** (A) AbGCs in their critical period exhibit greater spine turnover. (B) Left: MCs stimulated based on their location on a two-dimensional grid. Right: MCs initially respond similarly to both stimuli, but responses diverge after a 10 day enrichment. Over time, spontaneous synaptic changes lead to forgetting. (C) Top: Memory is measured as a function of the network connectivity (see methods) for three different models: neurons with fast plasticity (green), neurons with slow plasticity (blue), neurons with age-dependent plasticity (red). Dashed curves are networks without neurogenesis. Bottom: Memory is measured as a function of MC output activity (see Methods). The lines show the mean memory over eight trials, while the shaded areas show the range. (D) GCs were hierarchically clustered according to their connectivity. An example connectivity matrix and dendrogram is shown taken at the end of the enrichment period of one simulation. (E) AbGCs were split into groups based on the results of the clustering in (D): those with odor-specific clustering (orange) and those without (purple). GCs were plotted as a function of their birth-date relative to enrichment onset. Light grey shaded area: GCs who had their critical period overlap with the enrichment period. Dark grey area: GCs that start to silently integrate into the OB during enrichment.

fraction of mature GCs (non-shaded area) contributed to the memory. Notably, abGCs that arrived in the OB during the enrichment phase (dark grey area) made only a minimal contribution to the memory engram. This observation conflicts with experimental findings that the silencing of these abGCs extinguishes this memory [Forest et al., 2019, Forest et al., 2020]. However, we anticipated that this discrepancy could be reconciled by considering additional transient properties of abGCs, as we will explore in the sections below.

## 2.3 Age-dependent excitability enhances initial memories and the flexibility of the growing network

One aspect of GC development that may further encourage the preferential recruitment of young cells over mature ones is the increased excitability of young abGCs in their critical period (Figure 3A). We incorporate this into the model using an age-dependent parameter that governs excitability. Although abGCs that arrive in the OB during enrichment still fail to integrate with the stimulus (dark grey shaded area Figure 3B), we observe a greater preferential recruitment of young abGCs (grey shaded areas) to the learning cluster, enabling young abGCs to fully encode new information and allowing mature GCs to maintain their existing connectivity patterns.

Not only does age-dependent excitability provide more specific recruitment of GCs, but it also cooperates with the age-dependent plasticity to improve the initial memory of the OB. In fact, the enhanced excitability increases the initial memory in the network with age-dependent plasticity rates (Figure 3C, red curve) to the full strength of the fast network, while retaining the stability of the slow network.

Models of adult neurogenesis have a common drawback: as the networks grow, their performance tends to decrease due to greater interference by adult-born neurons [Aimone et al., 2011, Meltzer et al., 2005, Kudithipudi et al., 2022]. We hypothesized that the increased excitability of young abGCs may mitigate this effect by raising the activity of abGC synapses that would be otherwise quieted through lateral inhibition from the vast population of mature GCs. To test this, we conducted a simulation where the onset of enrichment was progressively delayed, allowing an increasing number of neurons to accumulate in the OB (Figure 3D). We carried out this simulation both with and without enhanced excitability in young abGCs. When the networks were small, the memory improved with the growing number of GCs in both cases. In larger networks, however, the learning capacity of the network declined substantially (Figure 3E). However, the network featuring age-dependent excitability consistently outperformed the network without this feature to the extent that it could still form a memory when the other network failed.

This is reflected in the connectivities shown in Figure 2F, where the colors of the subpanels correspond to the markers indicated in Figure 2E. At the time point marked by the red and blue boxes, both models recruit a large portion of GCs to learn the odors, but the GCs with enhanced excitability feature a denser connectivity to the odor-responding MCs. In the time point marked by the purple and yellow boxes, the GCs without enhanced excitability fail to learn, while a small number of GCs with enhanced excitability still develop an odor-specific connectivity. Thus, the transiently enhanced excitability of abGCs contributes to maintaining the learning flexibility of the OB in the face of persistent neurogenesis.

## 2.4 The silent integration of abGCs establishes latent memories

An important aspect of GC development that has yet to be computationally explored is the period of dendritic development when newborn neurons are integrating silently into the OB. Because of experimental evidence that elaboration of distal dendrites of abGCs is dependent on sensory input [Saghatelyan et al., 2005, Yoshihara et al., 2012a, Yoshihara et al., 2016], we biased the dendritic field of abGCs such that GCs are more likely to have potential synapses with MCs that were more active when the GC was 8-14 days old (Figure 4A). While this does not substantially affect any of the aforementioned properties of memories encoded by the network (Figure S2A), it allows the model to feature a more plausible level of dendritic sparsity while still maintaining performance (Figure 4B). More significantly, it leads to the preferential recruitment of abGCs that arrive in the OB during enrichment over those that arrive just before enrichment (Figure 4C, dark

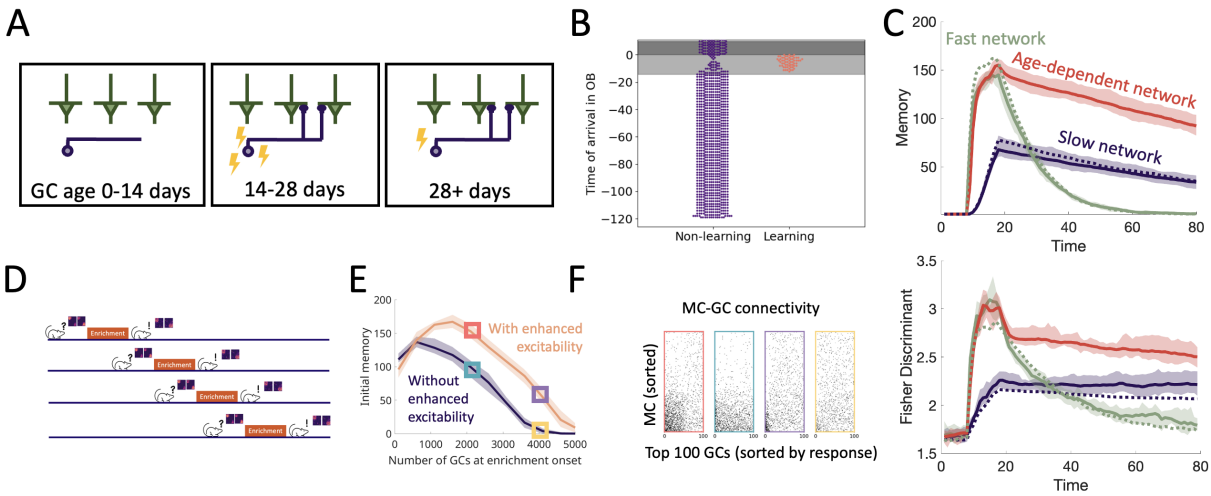


Figure 3: **Increased excitability.** (A) AbGCs exhibit increased excitability during their critical period. (B) The same birth-date analysis was performed as in 2E for data from the model featuring both age-dependent plasticity and excitability. (C) The same memory measurements were taken as in 2C. (D) Delayed enrichment simulation in which the model was allowed to grow for longer and longer times preceding enrichment. (E) The memory immediately following enrichment was plotted as a function of the number of GCs at enrichment onset for the case with (orange) and without (purple) age-dependent excitability. Lines show the mean of eight trials while the shaded area shows the full range of results. (F) Subsets of the connectivity matrix for example trials. GCs were ordered according to their average response to the stimuli. The connectivities of the top 100 GCs are shown for the cases marked with the corresponding color in (E).

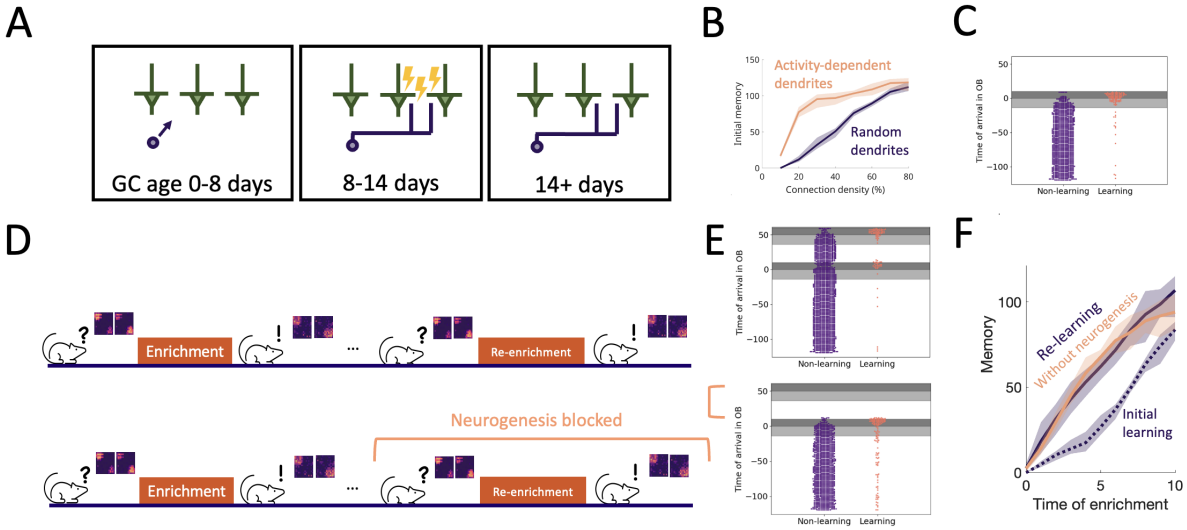


Figure 4: **Silent integration.** (A) Sensory-dependent silent integration of juvenile abGCs (see methods). (B) Memory following enrichment as a function of the dendritic sparsity with random (purple) and activity-dependent (orange) dendritic elaboration. (C) Birth-date analysis was repeated as in Figure 2E. (D) The model was exposed to an initial enrichment period, given time to forget what it learned and was then re-enriched with the same set of stimuli. (E) Birth-date analysis was repeated as in Figure 4C, including new light and dark grey bars corresponding to the re-enrichment period. (F) The evolution of memory during the initial enrichment (dotted line) and second enrichment both with (purple solid line) and without (orange solid line) neurogenesis. Lines show the average of eight trials and the shaded region shows the entire range of values.

grey area). This is consistent with experimental results showing that these abGCs encode the memory [Forest et al., 2019, Forest et al., 2020].

We also examine the savings effect [Ebbinghaus, 1885] in which the re-learning of forgotten information occurs more rapidly than the initial learning. Not only has this effect has been observed in associative olfactory learning task in rodents, but experimental data seem to implicate adult-neurogenesis as the driving factor [Sultan et al., 2010]. We examine this further in our perceptual learning framework by simulating a similar relearning experiment and exploring what happens if neurogenesis is blocked during relearning (Fig. 4D). The model predicts that GCs that initially encoded the memory are re-recruited to the odors during re-enrichment (Figure 4E). While these GCs are no longer as highly excitable or plastic as young GCs, they have the advantage over other GCs that their dendritic fields overlap strongly with MCs that are excited during enrichment, allowing them to more efficiently integrate with the enrichment odors. This leads to savings where the memory increases more rapidly during the second enrichment (Figure 4F). Additionally, we predict that savings will still be seen even if neurogenesis is blocked during the second enrichment (Figure 4E, F). Importantly, these observations do not occur without the activity-dependent dendritic elaboration of young abGCs (Figure S2B). In this sense, the dendrites encode "latent memories" that facilitate the rapid re-expression of a previously encoded memory upon re-exposure to the stimulus.

IN GIF>5C I **would reverse the xlable: 'Time abGCs arrived in OB'**

## 2.5 Targeted apoptosis maintains flexibility of the network

The final property of GC development that we investigate is the death of GCs through apoptosis. In the OB, apoptosis is believed to be activity-dependent [Lin et al., 2010] with young abGCs more susceptible than mature GCs [Yamaguchi and Mori, 2005]. Recently, however, the degree of apoptosis has become controversial as it has been revealed that in standard conditions without any olfactory stimuli or behavioral task, there is in fact very little observed apoptosis [Platel et al., 2019]. One potential explanation is that apoptosis is modulated by environmental and behavioral factors. Keeping with this, experiments have shown for example that survival of abGCs can be regulated by noradrenergic mechanisms in response to novel stimuli [Veyrac et al., 2009]. Furthermore it has been shown that apoptosis is more commonly observed during certain behavioral states [Yokoyama et al., 2011, Yamaguchi et al., 2013, Komano-Inoue et al., 2014], and, when triggered, is enhanced in GCs receiving fewer sensory inputs [Yokoyama et al., 2011]. Moreover, GC survival can be increased by increasing the intrinsic excitability of the cells and relies on NMDARs [Lin et al., 2010]. Together, these results indicate that apoptosis is dependent on activity and age of GCs, as well as the environment and internal state of the animal. Therefore as a minimal model of apoptosis, we assume all GCs have a low threshold of activity required for survival, leading to a low baseline rate of death, but olfactory enrichment leads to a apoptotic signal that increases the activity threshold of abGCs in their critical period (Figure 5A, Figure 1D).

We find that this leads to two noteworthy phenomena. First, when we track the growth of the network over time, we observe that the number of GCs initially grows approximately linearly, while growth eventually starts to slow (Figure 5B), as observed experimentally [Platel et al., 2019]. Second, in Figure 5C, we note that in response to olfactory enrichment there is a high rate of apoptosis in older young abGCs (light grey area) but not in abGCs that arrive in the OB during enrichment (dark grey area) or mature GCs (non-shaded area). This is similar to experimental results that show enhanced death of older young abGCs, but not young abGCs or more mature abGCs [Mouret et al., 2008].

What are the potential implications of apoptosis on memory encoding? One known outcome is that newly formed memories are subject to retrograde interference [Forest et al., 2019] (simulated in Figure S3). In these experiments, there were two enrichment periods with odors that activated largely non-overlapping sets of GCs. If the second enrichment occurred while abGCs that encoded the memory of the first enrichment were still in their critical period, then these abGCs succumbed to apoptosis and the memory was extinguished. Our model captures this and predicts that the near orthogonality of the odors is essential, since the connectivity devel-

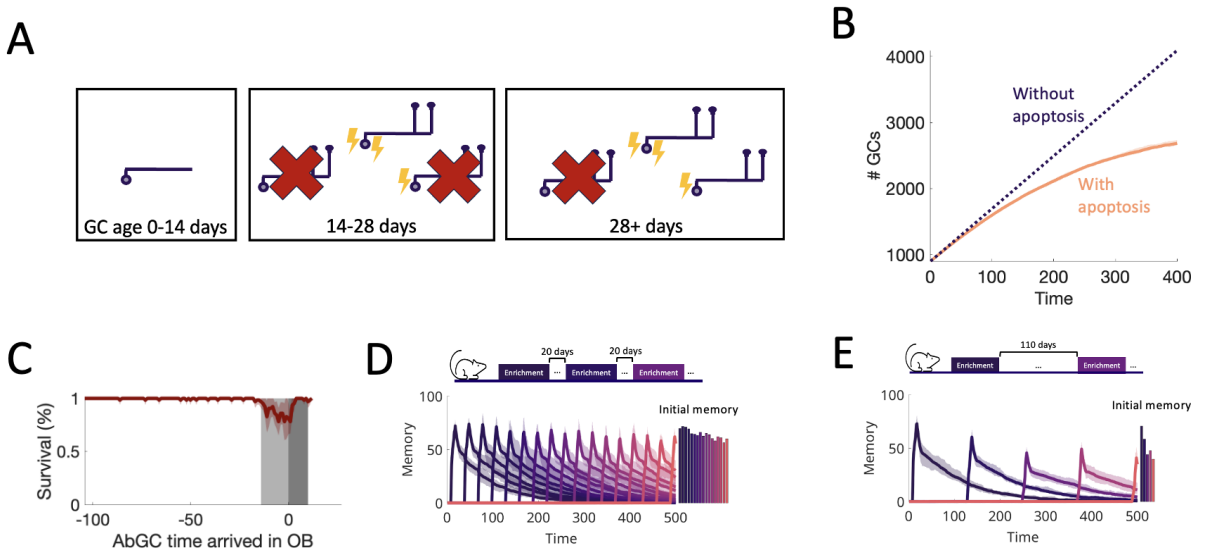


Figure 5: **Apoptosis**. (A) AbGCs in their critical period require a higher level of activity to survive. (B) The growth of the OB over time. (C) The portion of surviving GCs as a function of birth-date. The grey shaded regions are as in Figure 2E. The line shows the average over eight trials and the red shaded area shows the mean $\pm$ the standard deviation. (D, E) Sequential enrichment experiments differing in the inter-enrichment interval. Each curve corresponds to the memory of a stimulus pair. The bar plots show the mean initial memory for each enrichment period. The curves show the average over eight trials and the shaded areas show the range over all trials.

oped by the odor-encoding GCs during the first enrichment is odor-specific, these GCs are inactive during the second enrichment and therefore more susceptible to apoptosis (Fig S3). If, alternatively, there is a long enough gap between the enrichment periods, or if the odors from the first enrichment are present during the second enrichment then the abGCs encoding the first memory survive and the memory is consolidated in both the model and experiments. This highlights how apoptosis can selectively remove abGCs, and how only naive, young abGCs are available to encode new odors.

Yet the question still remains if apoptosis can facilitate the formation of new memories rather than exclusively eliminate old ones. Based on the observation in Figure 3 that the ability to form new memories declines as the number of GCs grows, and the observation in Figure 5B that apoptosis limits the rate of growth of the OB, we hypothesized that apoptosis may help sustain the flexibility of memory formation as adult neurogenesis persists. To test how well the network learns under different levels of apoptosis, we simulate an experiment where we give the network a variable number of equally-spaced enrichments consisting of sparse, uncorrelated odors over the same time interval (Figure 5D & E). Because enrichment clears a large portion of abGCs that are late in their critical period at enrichment onset (Figure 5C), we expect to see more apoptosis and thus improved learning in trials with a greater number of enrichments. Indeed, when there are many enrichments, the network flexibly learns all odors similarly well (Figure 5D), but when there are fewer enrichments, it loses flexibility as neurons accumulate in the OB (Figure 5E). As a result, the model predicts that long periods without olfactory enrichment negatively impacts the ability to learn new odors.

## 2.6 Adult neurogenesis supports life-long learning

To study the capacity of the OB to encode new stimuli continually over long periods of time, we simulated an experiment where we sequentially enrich the OB network on twenty-five sparse, random odor pairs (Figure 6A) and measure how the properties of the memories change over the course of time. We find that our full model of

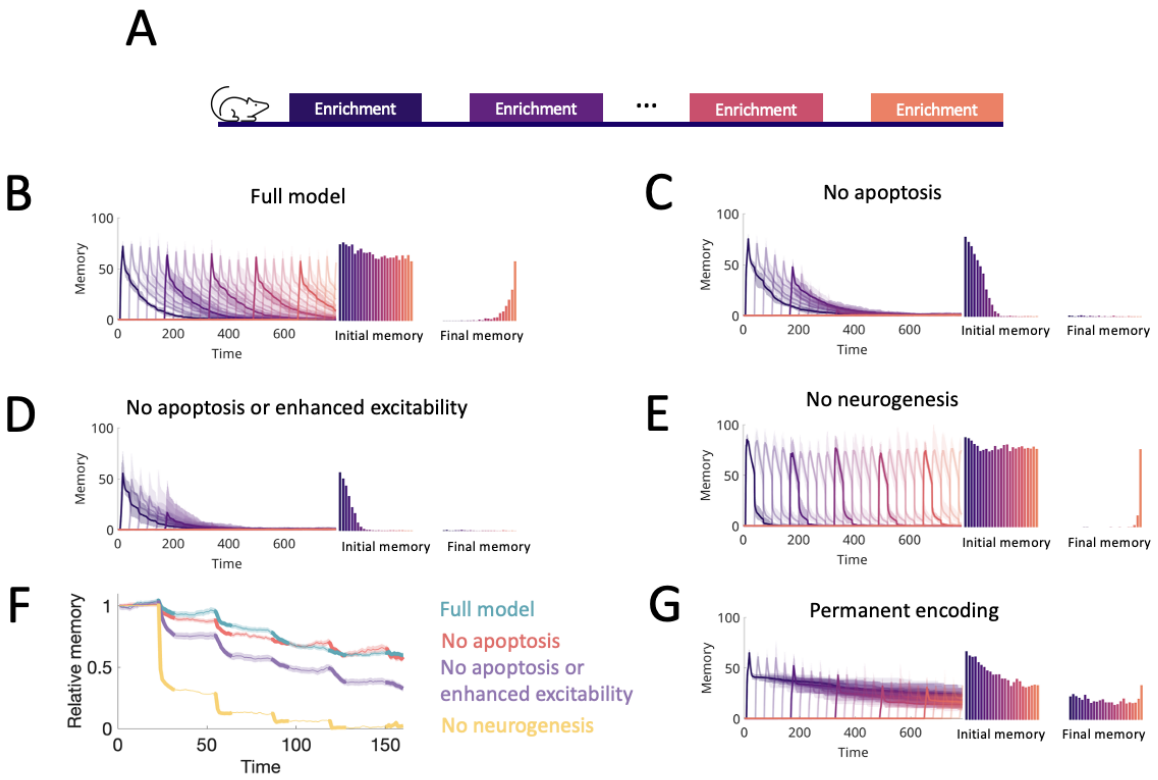


Figure 6: **Neurogenesis for lifelong learning.** (A) Protocol for sequential enrichment experiment. (B-E) Results of full model, model without apoptosis, model without apoptosis or age-dependent excitability, and a model without neurogenesis respectively. Each curve corresponds to the memory of a different set of stimuli, with every fifth curve bolded for visualization. The first bar plot plots show the mean initial memory, while the next bar plot shows the mean memory of at the end of the simulation. The curves show the average over eight trials and the shaded areas show the range over all trials. (F) The memory of the first enrichment in (B)-(E) is shown as a ratio of the memory trace of the model enriched with the same stimuli during the first enrichment but without any subsequent enrichment periods. The curves show the average relative memory over trials while the shaded area shows the standard error of the mean. Bolded segments correspond to times when there is a subsequent enrichment period. (G) Results of sequential enrichment simulation for a model in which mature abGCs have their connectivity frozen.

the OB supports the flexible encoding of stable memories (Figure 6B). Learning flexibility, measured as the initial memory of the enrichment odors, is strongest at the start of the simulation; it declines slightly in subsequent enrichments and approaches a steady value when the growth of the network starts to saturate. Additionally, memories remain stable as individual memory traces decay largely uninterrupted by subsequent, interfering enrichments. This results in multiple odors having substantial memories at the final time of measurement, and that these memories are graded according to the time of enrichment.

To show what properties of the OB are required to produce these results, we repeat the simulations under several different model conditions. First, in Figure 6C, we block apoptosis. While memories still remain stable, it is clear that flexibility suffers greatly as the network eventually fails to learn. Notably, the memories of early enrichments are not strongly impacted by this change in the model, indicating that short-term suppression of apoptosis should not affect learning, consistent with observations [Mouret et al., 2009]. Next, we additionally removed the enhanced excitability of young abGCs (Figure 6D). Not only did flexibility decline even more substantially, but memory stability also suffered as larger drops were evident in the individual memory traces during later enrichments. Finally, for comparison, we consider a non-neurogenic network featuring only synaptic plasticity and none of the transiently heterogeneous properties of abGCs (Figure 6E). While this network can flexibly form new memories, they are not stable as each subsequent enrichment leads to the overwriting of old memories, severely limiting the memory capacity.

To evaluate quantitatively how the memory formed in the first enrichment deteriorates due to the subsequent enrichments with other odors, we compare the memory trace of the first odor across the subsequent enrichments to the memory trace of the same odor, but without any subsequent enrichments. Taking the ratio between these two traces shows the extent that new stimuli overwrote old memories, shown in Figure 6F. As expected, the non-neurogenic model displayed the most overwriting, with prominent overwriting events during the first few enrichments. Next, the network without the transiently enhanced excitability of young abGCs featured a moderate amount of overwriting, as young abGCs were no longer preferentially recruited to learn new odors. Finally, the full model and the model without apoptosis featured similarly low levels of overwriting, indicating that apoptosis is required for memory flexibility but not stability.

Because of the low degree of overwriting occurring in our full model of the OB, memory decay is primarily due to spontaneous synaptic changes. This is embodied by the parameter $R_0$ that represents noise or unmodeled plasticity events. Notably, a large degree of spine turnover has been observed at MC-GC synapses in response to spontaneous activity alone even on mature GCs c [Livneh and Mizrahi, 2012, Sailor et al., 2016]. We investigated the implications of this large degree of plasticity in mature GCs with a model of the OB in which plasticity was prevented in older GCs. In that case new memories briefly decay due to spontaneous plasticity but then remain essentially unchanged for the duration of the simulation. Although there is explicitly no synaptic overwriting, the memories still feature a slow decay due to the apoptosis of odor-encoding GCs. Apoptosis is more prominent in this network because the odor-encoding neurons feature a larger number of synapses and thus exert more inhibition, making it more difficult for GCs to survive. Furthermore, these excess synapses lead to more interference which degrades the flexibility in this network (cf. initial memories in Figure 6B,G). This suggests that the strong synaptic fluctuations among mature GCs serve to increase flexibility by removing potentially interfering, un-maintained memories of odors. Of course, this strategy has the drawback that memories are less stable, but this drawback is mitigated by the latent memories of the odors being stored in the dendrites of abGCs, which allow for their rapid re-acquisition if the odors are once again present in the environment (Figure 4).

## 2.7 Age-dependent plasticity more efficiently utilizes the new synapses provided by adult-neurogenesis

From a signal-theoretic perspective, both initial strength and duration of a new memory should improve as synapses are added to the network. Due to the metabolic cost of forming and remov-

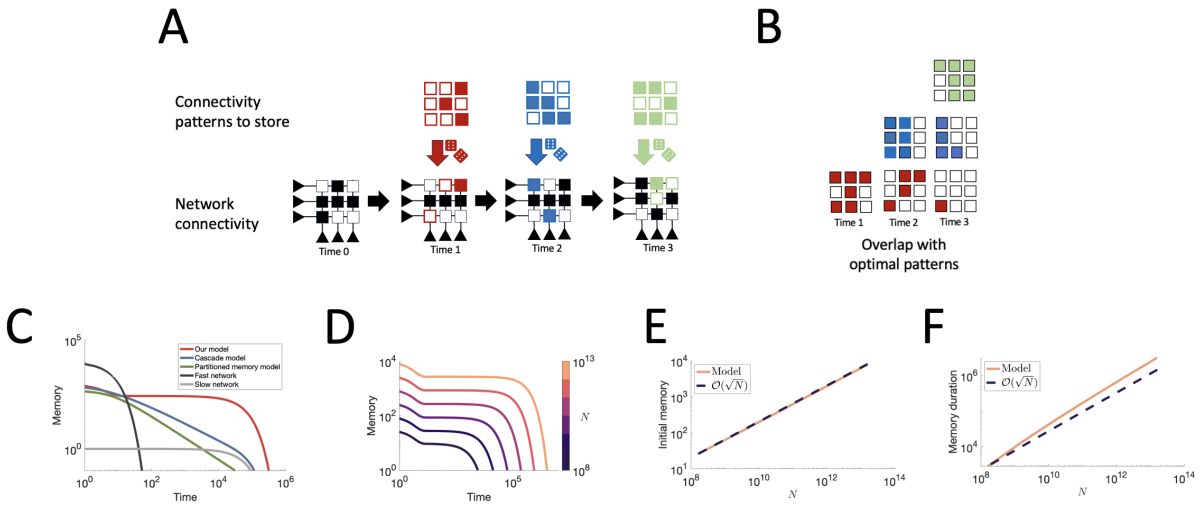


Figure 7: **Mean-field model.** (A) We assume there exists an optimal configuration that can process a given stimulus. In this framework, the network directly encodes this configuration stochastically according to the plasticity rate at each synapse, and at each time point a new stimulus is presented to the network. We track the memory of the network as the degree of overlap between the optimal network for a given stimulus and the current configuration of the network. B) Overlap between each stimulus and the current configuration of the network in (A). (C) Results of the mean-field approximation to the model described in (A) with age-dependent synaptic plasticity rates has similar initial memory and memory duration as the cascade model [Fusi et al., 2005], and the partitioned-memory model [Roxin and Fusi, 2013]. (D) Results of the age-dependent model for different values of the number of synapses $N$. (E) Initial memory as a function of $N$. (F) Memory duration as a function of $N$.

ing synapses it is important to use them efficiently. This is especially true for neurogenic systems in which the addition of synapses is to a large extent achieved by adding whole new neurons. The efficiency of the system can be characterized by how strongly its memory performance increases when the number $N$ of synapses is increased.

To assess the efficiency, we adapted a framework proposed by [Fusi et al., 2005, Roxin and Fusi, 2013] to analyze how memories degrade in response to ongoing plasticity. We considered a scenario where an ongoing stream of random, uncorrelated stimuli was presented to a network featuring binary synapses ('non-functional', 'functional'). Each stimulus independently initiated a candidate plasticity event (either consolidating or deconsolidating) each synapse. The synapses were correspondingly modified stochastically with a rate determined by the plasticity rate of the synapse (Figure 7A). To quantify memory performance, we tracked the signal-to-noise ratio ( SNR) of a single arbitrary stimulus immediately after stimulus presentation (the "initial memory" SNR(0)), as well as the time $T$ that it took for the SNR to decay to the value of 1 due to the storage of subsequent memories (the "memory lifetime") .

A mean-field approach for a system in which all synapses have only a single plasticity rate the initial memory strength SNR(0) would be given by $qN^{\frac{1}{2}}$ while the lifetime $T$ would be $q^{-1}\log(qN^{\frac{1}{2}})$ [Fusi et al., 2005, Roxin and Fusi, 2013] . The lifetime in such a system is maximized by slow learning, $q \sim N^{-\frac{1}{2}}$, which implies $T \sim N^{\frac{1}{2}}$, but results in a weak initial memory strength of $qN^{\frac{1}{2}} \propto 1$. Conversely, for fast learning, $q \sim 1$, the initial memory strength is $\sim N^{\frac{1}{2}}$ but the lifetime is only $\sim \log N^{\frac{1}{2}}$, exemplifying the stability-flexibility dilemma (black and gray lines in Figure 7C).

Motivated by our neurogenesis model, we consider a model with age-dependent plasticity rates in which most synapses have a small plasticity rate $q_1 \sim N^{-\frac{1}{2}}$. A smaller cohort, representing synapses on abGCs, initially have plasticity rate $q_2 \sim 1 \gg q_1$. As these abGCs mature, the plasticity rate of their synapses decreases to $q_1$. Because we track a single memory trace, we consider only a single cohort of new neurons; later cohorts have no impact on previously encoded memories in this framework. In this model, the synapses on the young abGCs provide an initial memory strength of approximately equal to $kq_2N^{\frac{1}{2}}$ where $k$ is the portion of initially highly plastic synapses (Figure 7D). The memory lifetime approximately follow $\frac{1}{q_1} = N^{\frac{1}{2}}$ (Figure 7E). Thus, like the cascade model and the partitioned-memory model, our age-dependent model effectively resolves the plasticity-flexibility dilemma, simultaneously achieving the greatest initial memory and memory duration possibly afforded by the homogeneous network with constant plasticity. Note that it is the age-dependent plasticity rate allowed by adult-neurogenesis, rather than the mere addition of synapses, that is responsible for the flexible encoding of stable memories. Furthermore this exhibits how new synapses are more efficiently used in the network.

# 3 Discussion

In this study, we show a clear computational advantage of adult-neurogenesis in continual memory encoding. In a computational model of the OB, the increased plasticity exhibited by abGCs in their critical period allows them to rapidly encode new information, while the subsequent development of these cells and the resulting decrease in plasticity rate ensures that the memories they encode remain stable. Meanwhile, the increased excitability of young abGCs enhances their preferential recruitment in learning new information, while also helping maintain the flexibility of the system as new neurons accumulate in the OB. Apoptosis similarly helps maintain learning flexibility through the targeted removal of abGCs that fail to learn the odors presented during their critical period. Furthermore, the silent integration of juvenile abGCs leads to pre-configured sub-networks of similarly aged abGCs that enable the rapid reacquisition of memory. We find that all of these elements are required to reproduce experimental results. Lastly, in a more general framework, we show that the age-dependent synaptic plasticity rates associated with the development of adult-born neurons makes more efficient use of the additional synapses than a network with static, homogeneous plasticity rates.

## 3.1 Other models addressing the flexibility-stability problem

Our findings contribute to the ongoing discourse on memory consolidation, adding a dimension to the existing body of research [Fusi et al., 2005, Roxin and Fusi, 2013, Benna and Fusi, 2016]. We demonstrated that networks comprising $N$ synapses with age-dependent plasticity rates exhibit an initial memory and memory duration on the order of $N^{\frac{1}{2}}$. This drastic improvement over networks with constant plasticity rate uncovers a new role of the plasticity mechanisms in the olfactory bulb as a method of memory consolidation. Our results are commensurate with previous consolidation models designed to address the flexibility-stability dilemma, as illustrated in Figure 7F, particularly the classical cascade model [Fusi et al., 2005] and the partitioned memory model of systems consolidation [Roxin and Fusi, 2013]. However, our model does not yield the $\mathcal{O}(N)$ memory duration demonstrated by the bidirectional cascade model [Benna and Fusi, 2016]. This difference underscores the intricate interplay of synaptic plasticity mechanisms and their impact on memory consolidation.

## 3.2 Why neurogenesis?

If there exist alternative methods that are theoretically demonstrated to consolidate memory with comparable effectiveness [Fusi et al., 2005, Roxin and Fusi, 2013, Benna and Fusi, 2016], why does the OB opt for adult neurogenesis? Adult neurogenesis is a rare phenomenon in mammals, but more common in organisms with less complex nervous systems, such as reptiles, birds, and fish. This contrast suggests an evolutionary pressure to reduce neurogenesis, a pressure that is resisted by the OB [Aimone, 2016]. To understand why neurogenesis is nevertheless favored in the OB, it is crucial to examine the specific function of the OB and its constituent GCs.

One of the observed functions of the OB is the enhancement of small differences between similar stimuli [Gschwend et al., 2015]. The lateral inhibition between MCs that is mediated by GCs plays a key role in this function [Wick et al., 2010, Wiechert et al., 2010, Koulakov et al., 2011],. This type of processing is similar to the contrast enhancement and edge enhancement performed in early visual processing by the retina [Hartline and Ratliff, 1957]. Since visual objects are always contiguous, the input that neighboring 'pixels' in the retina receive are quite strongly correlated, regardless of the specific visual scene. For such statistics, low-level processing of the stimuli is therefore possible with a pre-wired, spatially-dependent connectivity that provides interactions between spatially neighboring 'pixels'.

Olfactory stimuli, however, do not have this topographic correlation structure. Olfactory space is extremely high-dimensional, reflecting the large number of chemical odorants. Even if the activation patterns of similar olfactory stimuli differed only in neighboring 'olfactory pixels' in this high-dimensional space, their projection onto the two-dimensional arrangement of glomeruli would result in 'fragmented' activation patterns, wherein the relevant 'olfactory pixels' are widely distributed across large portions of the bulbar surface [**?**]; indeed, experiments have shown that the receptive fields of glomeruli are not informative of those of the nearby glomeruli [Soucy et al., 2009]. Therefore, seemingly random, spatially widespread 'olfactory pixels' exhibit correlations, and the specific set of correlated pixels will depend sensitively on the specific odor dominating the olfactory scene. Local processing in the glomerular layer can provide initial contrast enhancement [Cleland and Sethupathy, 2006]; however more finely-tuned secondary computations, such as odor learning, likely require mechanisms beyond local connectivity such as the lateral connectivity provided by GCs.

Only a subset of odors is innately relevant and has the same meaning for all animals of a given species. These odors can likely be processed with a fixed, pre-wired connectivity. However, odors that provide, e.g., kinship or pup recognition differ from individuum to individuum. Each animal must accordingly learn how to process these odors on-demand when they become relevant, which for many odors is not until the animal is mature. The OB must therefore allow for life-long learning.

For life-long learning, the flexible learning of new stimuli while maintaining the stability of old memories is crucial. Our modeling demonstrates that the neurogenesis and development of abGCs provides exactly this. However, we also show that both the survival of too many memo-

ries and of too many GCs can harm the flexibility of the network. This raises the question which memories and GCs should endure and for how long. Previous experiments and our modeling show that after an odor is learned, the abGCs recruited to that odor are subject to retrograde interference during their critical period: unless the initial odor is maintained in the environment the learning of a new memory decreases the survival of the abGCs associated with the earlier odor [Forest et al., 2019].

Past their critical period, the abGCs are much more stable. Nevertheless, the animals lose the memory of the learned odor over the course of 30-40 days [Forest et al., 2019]. However, at that point they can re-acquire that memory faster than they had learned it initially [Sultan et al., 2010]. This is consistent with the relevant synaptic connections being lost, reflecting the strong spontaneous formation and removal of GC spines [Sailor et al., 2016, Meng and Riecke, 2022], while the relevant GCs are still present and provide through their stable dendrites [Mizrahi, 2007, Sailor et al., 2016] a latent memory that can quickly be reactivated by reforming the relevant synapses.

What controls the survival of GCs over yet longer times is not quite clear. In [Sultan et al., 2010] the GCs die over the course of 90 days in the absence of the odor they memorized. In the experiments of [Platel et al., 2019], however, animals were not exposed to any tasks and little if any cell death is reported. From a functional point of view, the long-term survival of abGCs in the absence of the odor they have memorized is expected to be controlled on one hand by the need to avoid interference from unnecessary GCs and on the other hand by the possibility that the same odor will reappear at some later point in time. In principle, a sufficiently similar odor could become relevant, which would favor the persistence of these GCs. However, the vast dimension of odor space makes the latter quite unlikely and suggests that on a longer time scale GCs should be removed by apoptosis. Thus, our modeling suggests that the complexity of the odor activation pattern resulting from the high dimension of odor space together with the need for animals to learn specific such odors quickly but stably, even when they are already adult, strongly favors that adult neurogenesis and apoptosis that provide evolving structural synaptic plasticity.

## 3.3 Relation to adult neurogenesis in the hippocampus

Adult neurogenesis also occurs in the hippocampus where excitatory cells, also called granule cells, are persistently being born into the dentate gyrus [Kempermann et al., 2015, Christian et al., 2014]. Like olfactory abGCs, hippocampal abGCs exhibit age-dependent changes including increased plasticity and excitability in young cells [Lledo et al., 2006]. Unlike olfactory GCs, however, hippocampal GCs are excitatory and constitute the principal neurons of their network. Hippocampal GCs are thought to contribute to pattern separation and memory acquisition much like olfactory GCs, but also play an important role in other aspects of spatial and contextual memory [Christian et al., 2014, Aimone et al., 2009]. However, on the topic of memory stabilization, recent experiments have shown that up-regulating adult neurogenesis in the hippocampus can speed up the forgetting of previously learned information, while down-regulating adult neurogenesis can slow it down [Akers et al., 2014]. This suggests that interference from new cells makes old memories unstable and aids in memory clearance [Akers et al., 2014, Epp et al., 2016, Gao et al., 2018]. While neurogenesis also contributes noise to MC responses in our model, it is not so large that modifying the neurogenesis rate after learning would significantly alter the memory duration. Our research therefore suggests a different role for olfactory abGCs in this regard: their inhibitory nature may curtail interference to enhance memory stability rather than memory clearance.

## 3.4 The development of birthdate-dependent subnetworks

A key outcome of our model is the development of birthdate-dependent odor-specific subnetworks. This applies not only to the synaptic networks, but also to the underlying dendritic networks. In the model, this arises from the fact that abGCs born in a similar time window begin development in a similar environment. We therefore predict that the rapid re-learning observed in an olfactory associative learning task [Sultan et al., 2011] would also occur in a perceptual learning experiment and would still be

present even if neurogenesis was blocked after the initial enrichment.

This would be notable for two reasons. First, it has been shown that neurogenesis is required for perceptual learning of fine odor discrimination [Moreno et al., 2009], so if re-learning were to occur without neurogenesis then it would indicate that there is some structure storing a latent memory that is not expressed behaviorally. Second, this was not seen in the model without activity-dependent dendritic elaboration, so it would suggest that the dendritic tree may be a substrate of this latent memory. Importantly, these latent memories only persist as long as the neurons encoding them survive. It remains to be seen if periodic re-exposure to stimuli after learning can extend the lifetime of odor-encoding abGCs, as would be expected in a model where the OB predominantly eliminates GCs that encode extraneous information.

Similar results of birthdate-dependent subnetworks have been observed experimentally as a result of embryonic neurogenesis in the hippocampus [Huszar et al., 2022]. In this study, place cells in CA1 were observed to form assemblies where neurons were more likely to be in the same assembly with other neurons born on the same day compared to those born on different days. Importantly, in a place alternation task, these cells have also been observed to remap together, maintaining sub-assemblies across environments. In this sense, neurons exhibited a set of pre-configured activity patterns dependent on their birth-date, reminiscent of the latent memories we describe in our model.

## 3.5 The role of apoptosis in learning

In addition to predictions about relearning, the model predicts that enrichment-induced apoptosis helps maintain the flexibility of the OB (Figure 5D). In standard, non-enriched laboratory conditions, the observed rate of apoptosis of abGCs after they have established themselves in the OB network is low [Platel et al., 2019]. In such conditions, the model predicts that abGCs that fail to encode any relevant information accumulate in the OB and add non-specific inhibition to the OB, making it more difficult for new abGCs to integrate with new odors.

Olfactory enrichment eliminates many abGCs that are late in their critical period that may otherwise survive [Forest et al., 2019, Mouret et al., 2008]. At the same time, it also enhances the survival of a younger cohort of adult-born neurons [Rochefort et al., 2002]. The latter mechanism has not been built into the model, making it natural to wonder if this would impact the results in Figure 5. To address this, we doubled the neurogenesis rate during enrichment. This did not change the unsubstantial difference in results (Figure S4), in part due to the lower long-term survival of these neurons, as observed in [Rochefort and Lledo, 2005].

We expect that the enhanced flexibility due to apoptosis would be most pronounced in mice that are older than six months, but younger than twelve, when olfactory perceptual memory deficits start appearing [Greco-Vuilloud et al., 2022] and the growth of the granule cell layer starts to slow down [Platel et al., 2019]. Indeed, very recently it has been observed that long-term olfactory enrichment improves memory [Terrier et al., 2024].

Importantly, there are many other modulators of abGC survival beyond of olfactory enrichment. For example, apoptosis can be induced by a variety of behavioral states [Yokoyama et al., 2011, Yamaguchi et al., 2013, Komano-Inoue et al., 2014]. In the natural world we would therefore expect to see a more substantial degree of apoptosis, which the model predicts to preserve the flexibility of the OB.

## 3.6 Model Assumptions

As with all computational models, future experimental results may make it necessary to revisit certain assumptions made in the formulation of our model. Here, we assumed that there exists an explicit removal signal that enhances apoptosis under certain experimental conditions such as olfactory enrichment. While experiments have shown that top-down inputs in response to different environmental or behavioral state may provide such an apoptotic signal [Komano-Inoue et al., 2014, Yokoyama et al., 2011], how it precisely influences survival Ir ia nor knowqn, â. As a minimal model, we assumed that this signal shifts the survival curves (Figure 1D), but it is likely that apoptosis is a more complex process controlled by additional variables that are not yet well understood. Further investigation into the precise

biological mechanisms that regulate apoptosis in the OB would be needed to inform more detailed models.

In addition, the precise details of the maturation of adult-born neurons are not yet quite clear. For example, we have assumed that the age-dependent parameters follow a simple step function with the step occurring on day 28 for each parameter. While this assumption simplifies the model, the age-dependent properties of abGCs may change continuously over the course of development. Furthermore, it is not clear if experience alters the timeline of development by altering the critical periods of integration and survival. It is possible that inexperience may slow maturation, giving abGCs more time to integrate into the network or making them more more vulnerable to apoptosis in order to avoid wasting resources.

An important part of the processing of olfactory stimuli is the spike timing information, as experiments have shown that odor identity can be better decoded from spike timing than spike counts [Bolding and Franks, 2017]. Likewise, an important part of neural computation in general is the compartmentalization of the dendrites and soma. By modeling the activity of neurons with a single-compartment firing-rate model rather than a more complex spiking model, we neglect these important mechanisms and the information they convey. Our ideal observer approach of focusing on the network connectivity rather than the activity of the neurons circumvents this issue by providing an upper bound on the properties of memories in a more biologically plausible spiking model. Once sufficient information is available about the extent to which apoptosis depends on spiking dynamics a more refined model can be developed.

A prominent feature of olfaction is the extensive centrifugal input via top-down projections targeting GCs. Aside from the top-down apoptotic signal, we assumed that input from higher brain areas could be ignored for the perceptual learning tasks we explored here; however, it may play a larger role in other tasks such as those involving associated context [Mandairon et al., 2014]. Computational modeling [Adams et al., 2019] suggests that in such tasks, the bulbar component of the resulting learned connectivity features GCs developing odor-specific receptive fields with respect to their sensory and their top-down inputs. . In this case, the top-down inputs selectively activate GCs that, through their reciprocal connections with MCs, specifically modulate the bulbar response to the associated odor. The plasticity investigated here leads to a network with a similar connectivity structure in the bulb, which straightforwardly would provide the substrate for cortical control of odor processing by top-down inputs.

# 4 Methods

## 4.1 Neuron model

We model the activity of MCs and GCs within a firing-rate framework,

$$\tau_M \frac{dM_i}{dt} = -M_i + [S_i - \gamma \sum_j w_{i,j} G_j]_+, \quad (1)$$

$$\tau_G \frac{dG_i}{dt} = -G_i + r \sum_j w_{j,i} M_j. \quad (2)$$

Here, $M_i$ and $G_i$ represent the firing rates of individual mitral cells and granule cells, respectively, and $[x]_+$ denotes a threshold-linear rectifier: $[x]_+ = x$ for $x > 0$ and $[x]_+ = 0$ for $x \leq 0$. The input to MC $i$ consists of the sensory input $S_i^{odor}$ and a term $S^{spontaneous}$, through which the MCs have spontaneous activity even without sensory input,

$$S_i = S^{spontaneous} + S_i^{odor}. \quad (3)$$

The synaptic weights $w_{i,j}$ are 1 if the synapse between mitral cell $i$ and granule cell $j$ is fully functional and 0 otherwise. Note, that each synapse is reciprocal, with the strength of the inhibition by granule cells given by $\gamma$. The parameter $r$ captures the excitability of granule cells. Throughout this study we set the number of MCs $N_{MC}$ as 225, and the initial number of GCs $N_{GC}$ as 900.

To simulate neurogenesis, at each time step $N_{add}$ granule cells were added to the network. We chose $N_{add}$ to be 8 so that the ratio of new cells to existing cells would be consistent with experimental estimates [Kaplan et al., 1985]. These new neurons were immediately fully functional, corresponding in mice to abGCs that are about 14 days old [Kelsch et al., 2009, Carleton et al., 2003]. To reflect the observation that young abGCs, aged 14 to 28 days, are more

excitable than mature GCs, we made the parameter $r$ age-dependent. For simplicity, we assumed this age dependence followed a step function, such that young cells had a high level of excitability and mature cells had lower one (Table 1).

## 4.2 Network structure

Because a GC can only form synapses with MCs whose dendrites come physically close to the GC-dendrites, we impose the restriction that GCs can only make synapses with a predetermined set of $N_{conn}$ MCs. Since the MC dendrites extend across large portions of the olfactory bulb, we allowed connections between cells independent of their physical distance. For neonatal GCs, this subset was randomly chosen. For abGCs, however, starting in Section 2.4, this subset was chosen in a semi activity-dependent manner to reflect the activity-dependent and -independent mechanisms which guide dendritic growth in developing cells [Wong and Ghosh, 2002, Dahlen et al., 2011, Saghatelyan et al., 2005, Yoshihara et al., 2012b]. To this end, we calculate a variable, $\tilde{M}_{i,j}$ that is used to determine which MCs $i$ a given abGC $j$ can connect to:

$$\tilde{M}_{i,j} = [\bar{M}_i - \theta_M]_+ + \varepsilon_{i,j}. \tag{4}$$

Here, $\bar{M}_i$ is the average activity of MC $i$ over the 6 time steps preceding the birth of GC $j$ (corresponding to the amount of time between when an abGC arrives in the OB and when its starts spiking [Carleton et al., 2003]), $\theta_M$ is the threshold of activity required to induce dendritic growth, and $\varepsilon_{i,j}$ is a random variable that mimics the complex structure of the MC dendrites and a random position of the GC soma relative to the set of MCs when it starts developing its dendrite.

Whenever a GC $j$ is added to the network, the set $\{MC\}_j^{(pot)}$ of MCs to which it can connect is given by the $N_{conn}$ MCs that have the highest $\tilde{M}_{i,j}$ values at that time. Once a GC is added to the model, its set $\{MC\}_j^{(pot)}$ does not change; this is to reflect that dendrites of abGCs are relatively stable once the abGCs start spiking [Mizrahi, 2007, Sailor et al., 2016]. Lastly, when GC $j$ is added to the network it makes functional synapses with 10 MCs, randomly chosen from $\{MC\}_j^{(pot)}$. This applies to both neonatal and adult-born GCs.

## 4.3 Synaptic plasticity

We model synaptic dynamics as a Markov chain with three states: non-existent, unconsolidated, and consolidated. We include the unconsolidated state, since experimentally it is found that a substantial fraction of spines that are identified optically is lacking PSD-95 [Saha et al., 2021]. We assume state transitions from non-existent to unconsolidated occur randomly with a constant rate $\alpha$ and state transitions from unconsolidated to non-existent with constant rate $\beta$. Meanwhile, state transitions to and from the consolidated state rely on pre- and post-synaptic activity. This assumption is supported by experiments as it has been shown that GC spine dynamics depend on GC activity [Breton-Provencher et al., 2014, Breton-Provencher et al., 2016,
Saha et al., 2021]. Moreover, the formation and removal of consolidated synapses appear to be separate processes dependent on the calcium concentration at the synapse [Kasai et al., 2021, Stein et al., 2021, Park et al., 2021]. Therefore we express the rate $R^+_{i,j}$ for the consolidation of an unconsolidated synapse between MC $i$ and GC $j$ and the corresponding deconsolidation rate $R^-_{i,j}$ as functions of a variable $[Ca]_{i,j}$ that mimics the calcium concentration at the synapse,

$$R^+_{i,j} = R_0 + \frac{1}{2}(\tanh(([Ca]_{i,j} - \theta^+_j)) + 1) \tag{5}$$

$$R^-_{i,j} = R_0 + \frac{d}{\cosh(([Ca]_{i,j} - \theta^-_j))}. \tag{6}$$

$R_0$ is the rate of spontaneous spine changes, and $\theta^+_j$ and $\theta^-_j$ are parameters related to the thresholds of spine formation and removal specific to GC $j$. Additionally, $d$ is the relative rate of deconsolidation to consolidation, which we set to be less than one to reflect that consolidation is faster than deconsolidation [Kasai et al., 2021]. The functional forms of these equations were chosen to qualitatively resemble those of the Artola-Bröcher-Singer (ABS) rule of synaptic plasticity [Artola et al., 1990, Artola and Singer, 1993].

To model the local calcium concentration $[Ca]_{ij}$ at the synapse between MC $i$ and GC $j$, we adapt the model presented by [Graupner and Brunel, 2012] to our firing rate framework:

$$\tau \frac{d[Ca]_{ij}}{dt} = -[Ca]_{ij} + C_{pre} r M_i + C_{post} G_j. \tag{7}$$

Here $C_{pre}$ captures calcium influx driven by presynaptic activity: glutamatergic input from MC $i$ and the resulting depolarization within the spine of GC j allow calcium influx through NMDARs and voltage-gated calcium channels. $C_{post}$ captures calcium influx driven by post-synaptic activity that is independent of glutamate release from MC $i$ : depolarization in the spine that is driven by (global) spikes in the GC dendrite allows calcium influx through voltage-gated calcium channels. The global spikes are reflected in the activity of GC $j$ .

Next, we transform the rates $R^+_{i,j}$ and $R^-_{i,j}$ into state-transition probabilities through the functions

$$P^+_{ij} = 1 - \exp(-R^+_{i,j}), \tag{8}$$

$$P^-_{ij} = 1 - \exp(-R^-_{i,j}), \tag{9}$$

and stochastically consolidate synapses with probability $P^+_{ij}$ and deconsolidate synapses with probability $P^-_{ij}$.

In order to maintain stability of the network, we impose a sliding threshold rule on the local consolidation parameters $\theta^\pm_j$ ,

$$\theta^+_j = \max(\theta^+, k[\bar{Ca}]_j), \tag{10}$$

$$\theta^-_j = \max(\theta^-, k[\bar{Ca}]_j), \tag{11}$$

where $\theta^+$ and $\theta^-$ are the minimal thresholds for consolidation and deconsolidation respectively, $k$ is a parameter, and $[\bar{Ca}]_j$ is the calcium concentration averaged across GC $j$. The sliding threshold represents intracellular competition between synapses.

Lastly, we scale all synaptic transition rates $\alpha$, $\beta$, $R^+$ and $R^-$ by a common plasticity rate $p$ of the GC. To reflect the age-dependence of the plasticity rate, we make this parameter dependent on the age of each individual GC (see Table 1). The values of this parameter were chosen to match experimental data in [Sailor et al., 2016] that measure spine turnover in GCs of different ages.

## 4.4 Apoptosis

We model apoptosis as an activity-dependent process where neurons are removed stochastically with probability given by the sigmoid

$$\mathcal{P}_i = \frac{1}{2}(1 - \tanh(5(G_i - G_0))). \tag{12}$$

Here $\mathcal{P}_i$ is the apoptotic probability of granule cell $i$ and $G_0$ is an age-dependent survival threshold (Table 1). It reflects the fact that GCs are more susceptible to apoptosis in their critical period of survival [Yamaguchi and Mori, 2005], but still allows a small chance of apoptosis in mature GCs as observed experimentally [Yokoyama et al., 2011]. We model this by choosing the survival threshold $G_0$ to be higher for the immature abGCs than for the mature abGCs.

We also assume that a "removal signal" can cause young abGCs to be even more susceptible to apoptosis, raising the $G_0$ value for young cells further (Figure 1D). This assumption arises from the experimental finding that there is little observed cell death in GCs in standard conditions (even during their critical period) [Platel et al., 2019], but olfactory deprivation increases apoptosis across GC birthdates [Yamaguchi and Mori, 2005]. However, it has also been shown that apoptosis can be induced by certain behavioral states [Yamaguchi et al., 2013, Komano-Inoue et al., 2014, Yokoyama et al., 2011], and in such cases it is exacerbated in GCs receiving fewer sensory inputs [Yokoyama et al., 2011]. Furthermore, it has been shown that noradrenergic mechanisms active during olfactory enrichment can modulate apoptosis as well [Veyrac et al., 2009]. Based on these observations we assume that this "removal signal" is active only during enrichment.

## 4.5 Memory

To assess the ability of the model to learn, we introduce an anatomic memory measure that is based the network connectivity. Using an ideal observer approach, we assume that we have access to all synaptic strengths in the network. While the brain is unlikely to use such specific information to express memories, this gives us a limit on memory strength and duration and allows us to analyze how the OB network changes in response to olfactory enrichment.

We characterize the memory strength $\mu^s_i$ with which odor pair $s$ is 'memorized' by GC $i$ by the similarity (scalar product) between the average activity of MCs in response to that odor pair and the inhibition levied on those MCs by a unit ac-

tivation of the GC $i$,

$$\mu_i^s = \sum_{j=1}^{N_{MC}} w_{j,i} \bar{M}_j. \tag{13}$$

Here $\bar{M}_j$ is the mean activity of MC $j$ in response to both odors in the pair $s$. This reflects the fact that the plasticity processes of the model lead to a network connectivity that provides mutual inhibition between MCs reflecting their co-activity in response to the training stimuli. We use both odors in the pair $s$ to characterize the memory, since, throughout this study, we examine how the network is able to learn to discriminate between two similar odors, which are both presented to the network in an alternating fashion.

We then define the total memory $\mu^s$ of odor pair $s$ in the network as

$$\mu^s = \sum_{i=1}^{N_{GC}} [\mu_i^s - \theta_\mu(i)]_+. \tag{14}$$

Here, $\theta_\mu(i)$ is a threshold describing the "maximal null memory" of granule cell $i$. To obtain $\theta_\mu(i)$, we first determine the distribution of $\mu_i^s$ values for granule cell $i$ across a set of 10,000 reshuffled connectivities. Then we take $\theta_\mu(i)$ to be 3 standard deviations above the mean of this distribution. This provides us with a measure how well the odor pair is encoded in the network above what would be expected from a random connectivity.

## 4.6 Discriminability

In addition to using a connectivity-based learning measure, we use an activity-based learning measure to characterize to what extent learning enhances the ability of downstream cortical neurons to discriminate between the odors based on their read-out of the MC activities. Since the MC rate model does not include any fluctuations in activity, we assume that the rates represent the mean values of independent Poisson spike trains for which the variance is given by their mean. We assume a linear read-out of the MC activities with the weights chosen optimally and characterize the discriminability of stimulit $A$ and $B$ in terms of the optimal Fisher discriminant $F_{opt}$ [Adams et al., 2019],

$$F_{opt} = \sum_{i=1}^{N_{MC}} \frac{(M_i^{(A)} - M_i^{(B)})^2}{M_i^{(A)} + M_i^{(B)}}. \tag{15}$$

Thus, it can be seen that $F_{opt}$ will increase with the addition of MCs, reflecting the fact that even poorly discriminating MCs provide some additional information about the odors.

## 4.7 Clustering analysis

To characterize learning-induced subnetworks within the OB, we performed hierarchical clustering using an agglomerative approach with Ward linkage on the columns of the connectivity matrix between MCs and GCs [Pedregosa et al., 2011]. We then sought to identify the number of clusters present in the data using the resulting distances between groups of points returned by the algorithm. Due to the dependence of the clustering on the degree of the GCs, we did this using null distributions of the distances between groups found performing clustering on 10,000 shuffled networks, in the spirit of [Johnson et al., 2022]. This was done recursively. First we compared the distance between the two largest clusters in the data with the null distribution of distances between the largest clusters of shuffled data. If the true distance was outside of the distribution of shuffled distances then we deemed the cluster as significant and repeated the process on the two resulting subgroups. This continued until there were no new significant clusters.

## 4.8 Mean field Model

Following [Roxin and Fusi, 2013], we conceptualize a more general framework for studying perceptual memory. In this framework, we consider a network with $N$ binary synapses. At each time step, each synapse is independently presented with a plasticity event, which attempts to flip the synaptic strength depending on the presented stimulus and is accepted with probability $q_i$, the plasticity rate of synapse $i$. The presented stimuli are random and uncorrelated. Thus, on average the initial memory signal $\mu_i(t = 0)$ of a stimulus associated with synapse $i$ is $q_i$ and the total initial memory signal $\mu(0)$ of the network is

$$\mu(0) = \sum_{i=1}^{N} \mu_i(0) = \sum_{i=1}^{N} q_i. \tag{16}$$

Meanwhile, as this is a system of binomially distributed variables, the variance of the signal can be roughly approximated as $\sqrt{N}$

[Roxin and Fusi, 2013], leading to a signal-to-noise ratio $SNR(0)$ of

$$SNR(0) = \frac{1}{\sqrt{N}} \sum_{i=1}^{N} q_i. \tag{17}$$

As [Roxin and Fusi, 2013] show, the dynamics of the signal to noise ratio of the memory can be described by

$$\frac{dSNR}{dt} = \frac{1}{\sqrt{N}} \sum_{i=1}^{N} \frac{d\mu_i}{dt} \tag{18}$$

where the $\mu_i(t)$ follow the equations

$$\frac{d\mu_i}{dt} = -q_i \mu_i. \tag{19}$$

To incorporate the key element of our plasticity model we extend this model by making the plasticity rates $q_i$ depend on the ages of the cells such that

$$q_i = \begin{cases} q^{fast} & \text{if age of GC } i \text{ is} \leq T_c \text{ days} \\ q^{slow} & \text{if age of GC } i \text{ is} > T_c \text{ days,} \end{cases} \tag{20}$$

where $q^{fast} \gg q^{slow}$ and $T_c$ is the duration of the critical period during which the synapse is highly plastic. Following [Fusi et al., 2005], we chose $q^{fast} \sim \mathcal{O}(1)$ and $q^{slow} \sim \mathcal{O}(N^{-\frac{1}{2}})$. If, at the time of the stimulus presentation, the fraction of synapses on young GCs is $k$, then according to Eq.17 the $SNR$ of that memory is given by

$$SNR(0) = \sqrt{N}(kq^{fast} + (1-k)q^{slow}). \tag{21}$$

If $kq^{fast} \gg q^{slow}$, the initial memory is controlled by the fast plasticity rate, $SNR(0) \sim \sqrt{N}kq^{fast}$. Indeed, in the rat brain the total number of GCs is a few million, while roughly 10,000 more are born on each day [Kaplan et al., 1985]. Since the critical period lasts about 14 days, about 140,000 GCs have enhanced plasticity, so $k$ is on the order of 0.1. Thus assuming $N \sim 10^8$, $kq^{fast} \approx 10^{-1} \gg q^{slow} \approx 10^{-4}$ is a valid assumption.

The memory duration is determined by the time $T$ at which $SNR(t)$ falls below some fixed threshold $\theta_{SNR}$. Solving Eqs.17-20, we have that for $t \geq T_c$, $SNR(t)$ is given by

$$SNR(t) = \left[ q^{slow}(1-k)\sqrt{N} + q^{fast}\frac{k\sqrt{N}}{T_c} \sum_{j=0}^{T_c} e^{(q^{slow}-q^{fast})j} \right] e^{-q^{slow}t}. \tag{22}$$

We use this to solve for the memory duration $T$ where $SNR(T) = \theta_{SNR}$. Again, using $q^{slow} \sim \mathcal{O}(\frac{1}{\sqrt{N}})$ and $q^{fast} \sim \mathcal{O}(1)$ we get

$$T = \sqrt{N} \log \left[ \frac{1-k}{\theta_{SNR}} + \frac{k\sqrt{N}}{T_c \theta_{SNR}} \sum_{j=0}^{T_c} e^{(\frac{1}{\sqrt{N}}-1)j} \right]. \tag{23}$$

For large $N$, memory duration scales approximately as $T \sim \mathcal{O}(\sqrt{N}\log(\sqrt{N}))$, where the leading $\sqrt{N}$ arises from the inverse of $q^{slow}$. This shows that while initial memory is controlled by the fast plasticity of immature synapses, memory duration is controlled by the slow plasticity rate of mature synapses.

## 4.9 Robustness and parameters

The full list of parameters of the model and their default values is found in Tables 1 and 2. While many parameters were chosen by hand, several of them were fit quantitatively. For example, the parameters $C_{pre}$ and $C_{post}$ were fit using the genetic algorithm `ga` [The MathWorks Inc., 2022] to optimize memory following enrichment (Figure S5A). The parameters $\alpha$, $\beta$, and $p$ were fit to match the rates of spine turnover in young and mature abGCs found by [Sailor et al., 2016]. Meanwhile, some parameters were chosen to be consistent with more coarse experimental evidence. For example, $R_0$ controls memory decay due to spontaneous synaptic changes and was chosen such that memories endure for up to 30 days [Forest et al., 2019]. Since the forgetting may in part also be due to overwriting by other odors present, this value of $R_0$ may be somewhat too large. Additionally, the number of abGCs added each day, $N_{add}$ was chosen so that the ratio $\frac{N_{add}}{N_{CG}}$ matched experimental estimates [Kaplan et al., 1985]. Still, several parameters had to be chosen without any available experimental support. Below is a discussion of a few selected parameters and their impact on the simulations.

The first parameter the impact of which we assessed was the enhanced level of excitability of young abGCs, $r$. The initial memory was robust to changes in the parameter value, although learning declined slightly for the largest values we tested (Figure S5B). We next examine the model's dependence on the survival threshold of young abGCs, $G_0$ (Figure S5C). Trivially, if the threshold is too high then all new abGCs die before they can integrate into the network,

preventing learning; however, for lower thresholds learning is unaffected. In this regime, the primary difference is the survival rate of older young abGCs (grey shaded area).

We also explored the ramifications of changing the neurogenesis rate, $N_{add}$. Unsurprisingly, reducing the neurogenesis rate leads to weaker memories, but as $N_{add}$ is increased, the memory saturates (Figure S5D). Our choice of $N_{add}$ is in the saturated regime. The next parameter we tested was the parameter $k$ in the sliding threshold $\theta_j^{\pm}$. Compared to other parameters shown, small changes in $k$ (on the order of 20%) resulted in more significant changes. If $k$ was too small, GCs did not prune synapses that were not beneficial to processing the odors, leading to non-specific connectivity and poor learning (Figure S5E). Alternatively, if $k$ was too large, neurons started to have difficulty consolidating beneficial synapses, also harming learning.

The results were fairly robust to changes in the noise parameter $\epsilon$ that represents the activity independent component of dendritic elaboration. Most significantly, if the level of noise, represented by the width of the uniform distribution from which each $\epsilon$ was drawn, was too small, then the dendritic elaboration would be dominated by MC activity, forming permanent memories. In this scenario, GC dendrites would overlap almost exclusively with odor-responding MCs so that even if these GCs were connected with a random subset of those MCs, they would still encode a memory of the odor (Figure S5F). The final parameter we tested was the relative rate of consolidation to deconsolidation. Within the range we tested (50% - 150%), we saw no significant change in learning ability (Figure S5G), suggesting that this parameter does not substantially affect any of the results. This is significant because the precise value of this parameter is not well understood in the brain , though it is thought that deconsolidation is a slower process [Kasai et al., 2021].

# References


[Adams et al., 2019] Adams, W., Graham, J. N., Han, X., and Riecke, H. (2019). Top-down inputs drive neuronal network rewiring and context-enhanced sensory processing in olfaction. *PLoS Comp. Biology*, 15:e1006611.

[Aimone, 2016] Aimone, J. B. (2016). Computational modeling of adult neurogenesis. *Cold Spring Harbor perspectives in biology*, 8(4):a018960.

[Aimone et al., 2011] Aimone, J. B., Deng, W., and Gage, F. H. (2011). Resolving new memories: a critical look at the dentate gyrus, adult neurogenesis, and pattern separation. *Neuron*, 70(4):589–596.

[Aimone et al., 2009] Aimone, J. B., Wiles, J., and Gage, F. H. (2009). Computational influence of adult neurogenesis on memory encoding. *Neuron*, 61(2):187–202.

[Akers et al., 2014] Akers, K. G., Martinez-Canabal, A., Restivo, L., Yiu, A. P., De Cristofaro, A., Hsiang, H.-L. L., Wheeler, A. L., Guskjolen, A., Niibori, Y., Shoji, H., Ohira, K., Richards, B. A., Miyakawa, T., Josselyn, S. A., and Frankland, P. W. (2014). Hippocampal neurogenesis regulates forgetting during adulthood and infancy. *SCIENCE*, 344(6184):598–602.

[Amit and Fusi, 1994] Amit, D. J. and Fusi, S. (1994). Learning in neural networks with material synapses. *Neural Computation*, 6(5):957–982.

[Artola et al., 1990] Artola, A., Bröcher, S., and Singer, W. (1990). Different voltage-dependent thresholds for inducing long-term depression and long-term potentiation in slices of rat visual cortex. *Nature*, 347(6288):69–72.

[Artola and Singer, 1993] Artola, A. and Singer, W. (1993). Long-term depression of excitatory synaptic transmission and its relationship to long-term potentiation. *Trends in Neurosciences*, 16(11):480–487.

[Benna and Fusi, 2016] Benna, M. K. and Fusi, S. (2016). Computational principles of synaptic memory consolidation. *Nature neuroscience*, 19:1697–1706.

[Bolding and Franks, 2017] Bolding, K. A. and Franks, K. M. (2017). Complementary codes for odor identity and intensity in olfactory cortex. *eLife*, 6.

[Breton-Provencher et al., 2016] Breton-Provencher, V., Bakhshetyan, K., Hardy,

| | Immature cells | Mature cells | Description | Usage |
|---|---|---|---|---|
| $p$ | 0.2 | 0.02 | Plasticity rate | Scales $\alpha$, $\beta$, $R^+$, $R^-$ |
| $r$ | 1.5 | 1 | Excitability of GCs | Equations 2, 7 |
| $G_0$ | 3 (enriched), 0 (unenriched) | -0.45 | Survival threshold | Equation 12 |

Table 1: Age dependent parameters. GCs were considered immature if they were added to the network within 14 time steps, corresponding to their critical period.

| | Value | Description | Usage |
|---|---|---|---|
| $N_{MC}$ | 225 | Number of MCs | Network architecture |
| $N_{GC}$ | 900 | Initial number of GCs | Network architecture |
| $N_{add}$ | 8 | Number of GCs added each neurogenesis step | Network architecture |
| $N_{conn}$ | 30 | Number of MCs with which a GC can form synapses | Network architecture |
| $N_{init}$ | 10 | Number initial synapses made by each abGC | Network architecture |
| $\alpha$ | 0.08 | Rate of filopodia formation | Network architecture |
| $\beta$ | 1.5 | Rate of filopodia removal | Network architecture |
| $S^{spontaneous}$ | 0.1 | Spontaneous activity of sensory input | Equation 1 |
| $\gamma$ | 0.004 | Inhibitory strength of GCs | Equation 1 |
| $\theta^M$ | 0.15 | Threshold to induce dendritic growth | Equation 4 |
| $\epsilon_{i,j}$ | $\sim U(0, 1.3)$ | Noise in dendritic formation | Equation 4 |
| $R_0$ | 0.01 | Spontaneous rate of synaptic changes | Equations 5, 6 |
| $d$ | 0.7 | Relative rate of deconsolidation to consolidation | Equation 6 |
| $C_{pre}$ | 13.3 | Presynaptic calcium contribution | Equation 7 |
| $C_{post}$ | 4.3 | Postsynaptic calcium contribution | Equation 7 |
| $k$ | 0.95 | Consolidation threshold scalar | Equations 10, 11 |
| $\theta^+$ | 13.65 | Minimum threshold for consolidation | Equation 10 |
| $\theta^-$ | 13 | Minimum threshold for deconsolidation | Equation 11 |

Table 2: Age independent parameters used in the simulation of the model unless stated otherwise.

D., Bammann, R. R., Cavarretta, F., Snapyan, M., Cote, D., Migliore, M., and Saghatelyan, A. (2016). Principal cell activity induces spine relocation of adult-born interneurons in the olfactory bulb. *Nature communications*, 7:12659.

[Breton-Provencher et al., 2014] Breton-Provencher, V., Cote, D., and Saghatelyan, A. (2014). Activity of the principal cells of the olfactory bulb promotes a structural dynamic on the distal dendrites of immature adult-born granule cells via activation of nmda receptors. *The Journal of neuroscience : the official journal of the Society for Neuroscience*, 34:1748–1759.

[Carleton et al., 2003] Carleton, A., Petreanu, L. T., Lansford, R., Alvarez-Buylla, A., and Lledo, P. M. (2003). Becoming a new neuron in the adult olfactory bulb. *Nature Neurosc.*, 6(5):507–518.

[Chow et al., 2012] Chow, S. F., Wick, S. D., and Riecke, H. (2012). Neurogenesis drives stimulus decorrelation in a model of the olfactory bulb. *PLoS Comp. Biol.*, 8:e1002398.

[Christian et al., 2014] Christian, K. M., Song, H., and Ming, G.-l. (2014). Functions and dysfunctions of adult hippocampal neurogenesis. *Annual review of neuroscience*, 37:243–262.

[Cleland and Sethupathy, 2006] Cleland, T. A. and Sethupathy, P. (2006). Non-topographical contrast enhancement in the olfactory bulb. *BMC Neurosci.*, 7:7.

[Dahlen et al., 2011] Dahlen, J. E., Jimenez, D. A., Gerkin, R. C., and Urban, N. N. (2011). Morphological analysis of activity-reduced adult-born neurons in the mouse olfactory bulb. *Front Neurosci*, 5:66.

[Ebbinghaus, 1885] Ebbinghaus, H. (1885). *Über das gedächtnis: untersuchungen zur experimentellen psychologie*. Duncker & Humblot.

[Epp et al., 2016] Epp, J. R., Silva Mera, R., Köhler, S., Josselyn, S. A., and Frankland, P. W. (2016). Neurogenesis-mediated forgetting minimizes proactive interference. *Nature communications*, 7(1):10838.

[Forest et al., 2020] Forest, J., Chalencon, L., Midroit, M., Terrier, C., Caille, I., Sacquet, J., Benetollo, C., Martin, K., Richard, M., Didier, A., and Mandairon, N. (2020). Role of adult-born versus preexisting neurons born at p0 in olfactory perception in a complex olfactory environment in mice. *Cerebral cortex*, 30:534–549.

[Forest et al., 2019] Forest, J., Moreno, M., Cavelius, M., Chalencon, L., Ziessel, A., Sacquet, J., Richard, M., Didier, A., and Mandairon, N. (2019). Short-term availability of adult-born neurons for memory encoding. *Nature communications*, 10:5609.

[Fusi, 2021] Fusi, S. (2021). *Human Memory*, chapter Memory capacity of neural network models, page arXiv:2108.07839. Oxford University Press.

[Fusi and Abbott, 2007] Fusi, S. and Abbott, L. F. (2007). Limits on the memory storage capacity of bounded synapses. *Nature Neurosc.*, 10(4):485–493.

[Fusi et al., 2005] Fusi, S., Drew, P., and Abbott, L. (2005). Cascade models of synaptically stored memories. *Neuron*, 45(4):599–611.

[Gao et al., 2018] Gao, A., Xia, F., Guskjolen, A. J., Ramsaran, A. I., Santoro, A., Josselyn, S. A., and Frankland, P. W. (2018). Elevation of hippocampal neurogenesis induces a temporally graded pattern of forgetting of contextual fear memories. *Journal of Neuroscience*, 38(13):3190–3198.

[Gao and Strowbridge, 2009] Gao, Y. and Strowbridge, B. W. (2009). Long-term plasticity of excitatory inputs to granule cells in the rat olfactory bulb. *Nat Neurosci*, 12(6):731–733.

[Graupner and Brunel, 2012] Graupner, M. and Brunel, N. (2012). Calcium-based plasticity model explains sensitivity of synaptic changes to spike pattern, rate, and dendritic location. *Proceedings of the National Academy of Sciences of the United States of America*, 109(10):3991–3996.

[Greco-Vuilloud et al., 2022] Greco-Vuilloud, J., Midroit, M., Terrier, C., Forest, J., Sacquet, J., Mandairon, N., Didier, A., and Richard, M. (2022). 12 months is a pivotal age for olfactory perceptual learning and its underlying neuronal plasticity in aging mice. *Neurobiology of Aging*.

[Grossberg, 1982] Grossberg, S. (1982). Processing of expected and unexpected events udring conditionand and attention - a psychological theory. *Psychological review*, 89(5):529–572.

[Gschwend et al., 2015] Gschwend, O., Abraham, N. M., Lagier, S., Begnaud, F., Rodriguez, I., and Carleton, A. (2015). Neuronal pattern separation in the olfactory bulb improves odor discrimination learning. *Nature Neuroscience*, 18:1474–1482.

[Hartline and Ratliff, 1957] Hartline, H. K. and Ratliff, F. (1957). Inhibitory interaction of receptor units in the eye of limulus. *J. Gen. Physiol.*, 40(3):357–376.

[Huszar et al., 2022] Huszar, R., Zhang, Y., Blockus, H., and Buzsaki, G. (2022). Preconfigured dynamics in the hippocampus are guided by embryonic birthdate and rate of neurogenesis. *Nature Neuroscience*.

[Johnson et al., 2022] Johnson, E. M., Kath, W., and Mani, M. (2022). Embedr: Distinguishing signal from noise in single-cell omics data. *Patterns*, 3(3):100443.

[Kaplan et al., 1985] Kaplan, M. S., Mcnelly, N. A., and Hinds, J. W. (1985). Population-dynamics of adult-formed granule neurons of the rat olfactory-bulb. *J. Compar. Neurol.*, 239(1):117–125.

[Kasai et al., 2021] Kasai, H., Ziv, N. E., Okazaki, H., Yagishita, S., and Toyoizumi, T. (2021). Spine dynamics in the brain, mental disorders and artificial neural networks. *Nature reviews. Neuroscience*, 22:407.

[Kelsch et al., 2009] Kelsch, W., Lin, C.-W., Mosley, C. P., and Lois, C. (2009). A critical period for activity-dependent synaptic development during olfactory bulb adult neurogenesis. *J Neurosci*, 29(38):11852–11858.

[Kempermann et al., 2015] Kempermann, G., Song, H., and Gage, F. H. (2015). Neurogenesis in the adult hippocampus. *Cold Spring Harbor perspectives in biology*, 7(9):a018812.

[Kersen et al., 2022] Kersen, D. E. C., Tavoni, G., and Balasubramanian, V. (2022). Connectivity and dynamics in the olfactory bulb. *PLoS computational biology*, 18:e1009856.

[Komano-Inoue et al., 2014] Komano-Inoue, S., Manabe, H., Ota, M., Kusumoto-Yoshida, I., Yokoyama, T. K., Mori, K., and Yamaguchi, M. (2014). Top-down inputs from the olfactory cortex in the postprandial period promote elimination of granule cells in the olfactory bulb. *Eur J Neurosci*, 40(5):2724–2733.

[Koulakov et al., 2011] Koulakov, A. A., Kolterman, B. E., Enikolopov, A. G., and Rinberg, D. (2011). In search of the structure of human olfactory space. *Front. Syst. Neurosci.*, 5:65.

[Kudithipudi et al., 2022] Kudithipudi, D., Aguilar-Simon, M., Babb, J., Bazhenov, M., Blackiston, D., Bongard, J., Brna, A. P., Chakravarthi Raja, S., Cheney, N., Clune, J., Daram, A., Fusi, S., Helfer, P., Kay, L., Ketz, N., Kira, Z., Kolouri, S., Krichmar, J. L., Kriegman, S., Levin, M., Madireddy, S., Manicka, S., Marjaninejad, A., McNaughton, B., Miikkulainen, R., Navratilova, Z., Pandit, T., Parker, A., Pilly, P. K., Risi, S., Sejnowski, T. J., Soltoggio, A., Soures, N., Tolias, A. S., Urbina-MelÃ©ndez, D., Valero-Cuevas, F. J., van de Ven, G. M., Vogelstein, J. T., Wang, F., Weiss, R., Yanguas-Gil, A., Zou, X., and Siegelmann, H. (2022). Biological underpinnings for lifelong learning machines. *Nature Machine Intelligence*, 4(3):196–210.

[Li et al., 2018] Li, W. L., Chu, M. W., Wu, A., Suzuki, Y., Imayoshi, I., and Komiyama, T. (2018). Adult-born neurons facilitate olfactory bulb pattern separation during task engagement. *eLife*, 7.

[Lin et al., 2010] Lin, C.-W., Sim, S., Ainsworth, A., Okada, M., Kelsch, W., and Lois, C. (2010). Genetically increased cell-intrinsic excitability enhances neuronal integration into adult brain circuits. *Neuron*, 65:32–9.

[Livneh and Mizrahi, 2012] Livneh, Y. and Mizrahi, A. (2012). Experience-dependent plasticity of mature adult-born neurons. *Nat Neurosci*, 15(1):26–28.

[Lledo et al., 2006] Lledo, P. M., Alonso, M., and Grubb, M. S. (2006). Adult neurogenesis and functional plasticity in neuronal circuits. *Nature Rev. Neurosc.*, 7(3):179–193.

[Mandairon et al., 2014] Mandairon, N., Kermen, F., Charpentier, C., Sacquet, J., Linster,

C., and Didier, A. (2014). Context-driven activation of odor representations in the absence of olfactory stimuli in the olfactory bulb and piriform cortex. *Front Behav Neurosci*, 8:138.

[McNamara et al., 2008] McNamara, A. M., Magidson, P. D., Linster, C., Wilson, D. A., and Cleland, T. A. (2008). Distinct neural mechanisms mediate olfactory memory formation at different timescales. *Learning & Memory*, 15(3):117–125.

[Meltzer et al., 2005] Meltzer, L. A., Yabaluri, R., and Deisseroth, K. (2005). A role for circuit homeostasis in adult neurogenesis. *Trends Neurosci.*, 28(12):653–660.

[Meng and Riecke, 2022] Meng, J. H. and Riecke, H. (2022). Structural spine plasticity: Learning and forgetting of odor-specific subnetworks in the olfactory bulb. *PLOS Computational Biology*, 18(10):1–30.

[Mizrahi, 2007] Mizrahi, A. (2007). Dendritic development and plasticity of adult-born neurons in the mouse olfactory bulb. *Nat Neurosci*, 10(4):444–452.

[Moreno et al., 2009] Moreno, M. M., Linster, C., Escanilla, O., Sacquet, J., Didier, A., and Mandairon, N. (2009). Olfactory perceptual learning requires adult neurogenesis. *Proc Natl Acad Sci U S A*, 106(42):17980.

[Mouret et al., 2008] Mouret, A., Gheusi, G., Gabellec, M., de Chaumont, F., Olivo-Marin, J., and Lledo, P. (2008). Learning and survival of newly generated neurons: when time matters. *J Neurosci*, 28(45):11511–11516.

[Mouret et al., 2009] Mouret, A., Lepousez, G., Gras, J., Gabellec, M.-M., and Lledo, P.-M. (2009). Turnover of newborn olfactory bulb neurons optimizes olfaction. *J Neurosci*, 29(39):12302–12314.

[Nissant et al., 2009] Nissant, A., Bardy, C., Katagiri, H., Murray, K., and Lledo, P.-M. (2009). Adult neurogenesis promotes synaptic plasticity in the olfactory bulb. *Nat Neurosci*, 12(6):728–730.

[Park et al., 2021] Park, D. K., Petshow, S., Anisimova, M., Barragan, E. V., Gray, J. A., Stein, I. S., and Zito, K. (2021). Non-ionotropic nmda receptor signaling alters structural plasticity of dendritic spines in a mouse model for studying schizophrenia. *bioRxiv*.

[Pedregosa et al., 2011] Pedregosa, F., Varoquaux, G., Gramfort, A., Michel, V., Thirion, B., Grisel, O., Blondel, M., Prettenhofer, P., Weiss, R., Dubourg, V., Vanderplas, J., Passos, A., Cournapeau, D., Brucher, M., Perrot, M., and Duchesnay, E. (2011). Scikit-learn: Machine learning in Python. *Journal of Machine Learning Research*, 12:2825–2830.

[Platel et al., 2019] Platel, J.-C., Angelova, A., Bugeon, S., Wallace, J., Ganay, T., Chudotvorova, I., Deloulme, J.-C., Beclin, C., Tiveron, M.-C., Core, N., Murthy, V. N., and Cremer, H. (2019). Neuronal integration in the adult mouse olfactory bulb is a non-selective addition process. *eLife*, 8:e44830.

[Rochefort et al., 2002] Rochefort, C., Gheusi, G., Vincent, J. D., and Lledo, P. M. (2002). Enriched odor exposure increases the number of newborn neurons in the adult olfactory bulb and improves odor memory. *J. Neurosci.*, 22(7):2679–2689.

[Rochefort and Lledo, 2005] Rochefort, C. and Lledo, P. M. (2005). Short-term survival of newborn neurons in the adult olfactory bulb after exposure to a complex odor environment. *Eur. J. Neurosci.*, 22(11):2863–2870.

[Roxin and Fusi, 2013] Roxin, A. and Fusi, S. (2013). Efficient partitioning of memory systems and its importance for memory consolidation. *PLoS Comput Biol*, 9(7):e1003146.

[Saghatelyan et al., 2005] Saghatelyan, A., Roux, P., Migliore, M., Rochefort, C., Desmaisons, D., Charneau, P., Shepherd, G., and Lledo, P. (2005). Activity-dependent adjustments of the inhibitory network in the olfactory bulb following early postnatal deprivation. *Neuron*, 46(1):103–116.

[Saha et al., 2021] Saha, S., Meng, J. H., Riecke, H., Agoranos, G., Sailor, K. A., and Lledo, P.-M. (2021). Interneuron activity-structural plasticity association is driven by context-dependent odor experience. *bioRxiv 2021.01.28.428612*.

[Sailor et al., 2016] Sailor, K. A., Valley, M. T., Wiechert, M. T., Riecke, H., Sun, G. J., Adams, W., Dennis, J. C., Sharafi, S., Ming, G.-L.,

Song, H., and Lledo, P.-M. (2016). Persistent structural plasticity optimizes sensory information processing in the olfactory bulb. *Neuron*, 91(2):384–396.

[Shani-Narkiss et al., 2020] Shani-Narkiss, H., Vinograd, A., Landau, I. D., Tasaka, G., Yayon, N., Terletsky, S., Groysman, M., Maor, I., Sompolinsky, H., and Mizrahi, A. (2020). Young adult-born neurons improve odor coding by mitral cells. *Nature communications*, 11:5867.

[Soucy et al., 2009] Soucy, E. R., Albeanu, D. F., Fantana, A. L., Murthy, V. N., and Meister, M. (2009). Precision and diversity in an odor map on the olfactory bulb. *Nat Neurosci*, 12(2):210–220.

[Stein et al., 2021] Stein, I. S., Park, D. K., Claiborne, N., and Zito, K. (2021). Non-ionotropic nmda receptor signaling gates bidirectional structural plasticity of dendritic spines. *Cell Reports*, 34(4):108664.

[Sultan et al., 2011] Sultan, S., Lefort, J. M., Sacquet, J., Mandairon, N., and Didier, A. (2011). Acquisition of an olfactory associative task triggers a regionalized down-regulation of adult born neuron cell death. *Front Neurosci*, 5:52.

[Sultan et al., 2010] Sultan, S., Mandairon, N., Kermen, F., Garcia, S., Sacquet, J., and Didier, A. (2010). Learning-dependent neurogenesis in the olfactory bulb determines long-term olfactory memory. *Faseb J.*, 24(7):2355–2363.

[Terrier et al., 2024] Terrier, C., Greco-Vuilloud, J., Cavelius, M., Thevenet, M., Mandairon, N., Didier, A., and Richard, M. (2024). long-term olfactory enrichment promotes non-olfactory cognition, noradrenergic plasticity and remodeling of brain functional connectivity in older mice. *Neurobiology of Aging*.

[The MathWorks Inc., 2022] The MathWorks Inc. (2022). Optimization toolbox version: 9.4 (r2022b).

[Vardalaki et al., 2022] Vardalaki, D., Chung, K., and Harnett, M. T. (2022). Filopodia are a structural substrate for silent synapses in adult neocortex. *Nature*, 612(7939):323–327.

[Veyrac et al., 2009] Veyrac, A., Sacquet, J., Nguyen, V., Marien, M., Jourdan, F., and Didier, A. (2009). Novelty determines the effects of olfactory enrichment on memory and neurogenesis through noradrenergic mechanisms. *Neuropsychopharmacology*, 34(3):786–795.

[Wallace et al., 2017] Wallace, J. L., Wienisch, M., and Murthy, V. N. (2017). Development and refinement of functional properties of adult-born neurons. *Neuron*.

[Wick et al., 2010] Wick, S., Wiechert, M., Friedrich, R., and Riecke, H. (2010). Pattern orthogonalization via channel decorrelation by adaptive networks. *J Comput Neurosci*, 28:29–45.

[Wiechert et al., 2010] Wiechert, M. T., Judkewitz, B., Riecke, H., and Friedrich, R. W. (2010). Mechanisms of pattern decorrelation by recurrent neuronal circuits. *Nat Neurosci*, 13(8):1003–1010.

[Wong and Ghosh, 2002] Wong, R. O. L. and Ghosh, A. (2002). Activity-dependent regulation of dendritic growth and patterning. *Nat. Rev. Neurosci.*, 3:803–812.

[Yamaguchi et al., 2013] Yamaguchi, M., Manabe, H., Murata, K., and Mori, K. (2013). Reorganization of neuronal circuits of the central olfactory system during postprandial sleep. *Front Neural Circuits*, 7:132.

[Yamaguchi and Mori, 2005] Yamaguchi, M. and Mori, K. (2005). Critical period for sensory experience-dependent survival of newly generated granule cells in the adult mouse olfactory bulb. *Proc Natl Acad Sci U S A*, 102(27):9697–9702.

[Yokoyama et al., 2011] Yokoyama, T. K., Mochimaru, D., Murata, K., Manabe, H., Kobayakawa, K., Kobayakawa, R., Sakano, H., Mori, K., and Yamaguchi, M. (2011). Elimination of adult-born neurons in the olfactory bulb is promoted during the postprandial period. *Neuron*, 71(5):883–897.

[Yoshihara et al., 2012a] Yoshihara, S.-i., Takahashi, H., Nishimura, N., Naritsuka, H., Shirao, T., Hirai, H., Yoshihara, Y., Mori, K., Stern, P. L., and Tsuboi, A. (2012a). 5t4 glycoprotein regulates the sensory input-dependent development of a specific subtype of newborn interneurons in the mouse

olfactory bulb. *Journal of Neuroscience*, 32(6):2217–2226.

[Yoshihara et al., 2012b] Yoshihara, S.-i., Takahashi, H., Nishimura, N., Naritsuka, H., Shirao, T., Hirai, H., Yoshihara, Y., Mori, K., Stern, P. L., and Tsuboi, A. (2012b). 5t4 glycoprotein regulates the sensory input-dependent development of a specific subtype of newborn interneurons in the mouse olfactory bulb. *Journal of Neuroscience*, 32(6):2217–2226.

[Yoshihara et al., 2016] Yoshihara, S.-i., Takahashi, H., and Tsuboi, A. (2016). Molecular mechanisms regulating the dendritic development of newborn olfactory bulb interneurons in a sensory experience-dependent manner. *FRONTIERS IN NEUROSCIENCE*, 9.